RESEARCH MEMORANDUM

SOME ASPECTS OF THE DESIGN OF HYPERSONIC BOOST-GLIDE AIRCRAFT

By Alvin Seiff and H. Julian Allen

Ames Aeronautical Laboratory
Moffett Field, Calif.

NATIONAL ADVISORY COMMITTEE
FOR AERONAUTICS

WASHINGTON
August 15, 1955

1M

NATIONAL ADVISORY COMMITTEE FOR AERONAUTICS

RESEARCH MEMORANDUM

SOME ASPECTS OF THE DESIGN OF HYPERSONIC BOOST-GLIDE AIRCRAFT

By Alvin Seiff and H. Julian Allen

SUMMARY

Factors influencing flight range and aerodynamic heating for hypersonic boost-glide aircraft are discussed. It is shown that the blunting required to reduce aerodynamic heating at the wing leading edge to a tolerable level is detrimental to flight range but that by employing leading-edge sweepback this detrimental effect may largely be avoided. The possibility and advantages of flight at very high altitude to reduce aerodynamic heating and encourage the preservation of laminar flow on the surfaces of such aircraft is treated. One aircraft configuration is described and discussed as an example.

INTRODUCTION

Sanger (ref. 1) was among the first to give serious consideration to the use of winged high-velocity rockets for long-range flight and, with Bredt (ref. 2), to the use of such hypervelocity vehicles as man-carrying aircraft. They showed that two types of such vehicles were promising as regards efficiency of flight: The first, known as the boost-glide vehicle, is one which is boosted to its maximum speed and to an altitude such that at burnout the dynamic pressure is that required for flight at the lift coefficient corresponding to maximum lift-drag ratio for the vehicle. The unpowered flight is continuously maintained at maximum lift-drag ratio, the altitude decreasing as the vehicle is retarded under the action of aerodynamic drag, until near the end of flight the vehicle lift coefficient is increased to that required to effect a low-speed landing. The second, known as the boost-skip vehicle, is one which is boosted to its maximum speed along a ballistic trajectory. As the vehicle returns to earth at the end of the first ballistic phase of flight it enters the atmosphere and at maximum lift-drag ratio turns upward (i.e., "skips" from the atmosphere) into the second ballistic phase of flight. This combined ballistic and skipping trajectory is continued until the total energy available for flight is just sufficient to effect a landing.

Ballistic rockets as well as the boost-glide and boost-skip vehicles are of interest for military application because of their relative invulnerability as compared to other forms of aircraft. For manned flight,

[redacted]

[redacted]

however, only the glide and skip vehicles appear suitable for consideration. The efficiency of flight of glide and skip vehicles has been considered in reference 3 and has been compared with conventional supersonic airplanes. In that analysis it was shown that for long-range flight, both the rocket-powered glide and skip vehicles can compare favorably in efficiency with turbojet- or ramjet-powered supersonic airplanes designed to operate at Mach numbers for which obtainable lift-drag ratios are of the same order as those obtainable for the hypervelocity vehicles. The analysis of reference 3 indicates that for a given lift-drag ratio the skip vehicle is superior to the glide vehicle in the sense that for a given vehicle velocity at burnout the range is greater. However, it was noted that the superiority in this regard is slight for lift-drag ratios of 4 and more and it was concluded that the skip vehicle, for which the aerodynamic heating problems are very severe, is probably inferior to the glide vehicle when all factors are considered. Such a conclusion is particularly warranted in the case of a manned vehicle since the optimum skip vehicle for long-range flight must, in addition, experience very large accelerations during the skipping process. Thus, of the three hypervelocity vehicles considered, only the boost-glide type appears suitable for manned flight, but even this vehicle will be of limited usefulness since it cannot be a very maneuverable vehicle in the usual sense and thus is, perhaps, limited to use for bombing and reconnaissance. If the boost-glide vehicle is to compete favorably with the supersonic airplane, it is mandatory that the highest possible lift-drag ratios be obtained and that the aerodynamic heating be a minimum. It is the purpose of this paper to discuss these two aspects of design for the hypervelocity boost-glide vehicle.

SYMBOLS

b	span
C	constant
C_D	drag coefficient
$C_{D_{le}}$	coefficient of drag due to leading-edge rounding
C_{D_o}	minimum drag coefficient
$C_{D_{opt}}$	drag coefficient at maximum lift-drag ratio
C_L	lift coefficient
$C_{L_{opt}}$	lift coefficient at maximum lift-drag ratio
c_f	friction drag coefficient

c_{f_i}	friction drag coefficient for incompressible flow
D	drag
d	maximum body diameter
g	acceleration due to gravity
H	heat transferred by convection per unit area
h	convective heat-transfer coefficient
I	rocket specific impulse
K	constant
k	air thermal conductivity
L	lift
$\frac{L}{D}$	lift-drag ratio
$\left(\frac{L}{D}\right)_{opt}$	optimum (maximum) lift-drag ratio
l	length
M	Mach number
m	mass
m_o	initial mass
m_b	mass at rocket "burnout"
n	permissible acceleration for a man in terms of g
Pr	Prandtl number
p	static pressure
p_l	lower-surface pressure
p_u	upper-surface pressure
R	free-stream length Reynolds number
R_l	lower-surface length Reynolds number

[redacted]

R_u	upper-surface length Reynolds number
r	flight altitude as measured from earth's center
r_o	radius of the earth
r_c	flight-path radius of curvature
S	wing area
St	Stanton number
s	distance along flight path
T	rocket thrust
T_r	recovery temperature
T_w	airplane surface temperature
t	time
V	flight velocity (assumed also to be wing surface velocity at zero lift)
V_b	"burnout" velocity
V_l	lower surface air velocity
V_s	satellite speed (25,930 ft/sec)
V_u	upper-surface air velocity
W	weight
X	total flight range
X_p	range during powered flight
X_u	range during unpowered flight
y	altitude measured from earth's surface
α	angle of attack
α_{opt}	angle of attack for maximum lift-drag ratio
β	$\sqrt{M^2 - 1}$

γ	ratio of specific heats
ϵ	emissivity for radiation
θ	flight-path angle of descent
Λ	leading-edge sweepback angle
μ	air-stream viscosity
μ_l	air viscosity at boundary-layer edge on lower surface of wing
μ_u	air viscosity at boundary-layer edge on upper surface of wing
ξ	angle-of-attack factor, $\beta\alpha$
ξ_{opt}	angle-of-attack factor, $\beta\alpha_{opt}$
ρ	air-stream density
ρ_l	air density at boundary-layer edge on lower surface of wing
ρ_u	air density at boundary-layer edge on upper surface of wing
σ	leading-edge radius
ψ	angular range to go (see eqs. (2))

DESIGN CONSIDERATIONS

The Range Equation

Consider a boost-glide vehicle in gliding flight at velocity V as shown in the sketch. Following the analysis of reference 3, the parametric equations of force normal and parallel to the direction of motion are

$$\left.\begin{aligned} L - mg\cos\theta &= -\frac{mV^2}{r_c} \\ -D + mg\sin\theta &= m\frac{dV}{dt} \end{aligned}\right\} \qquad (1)$$

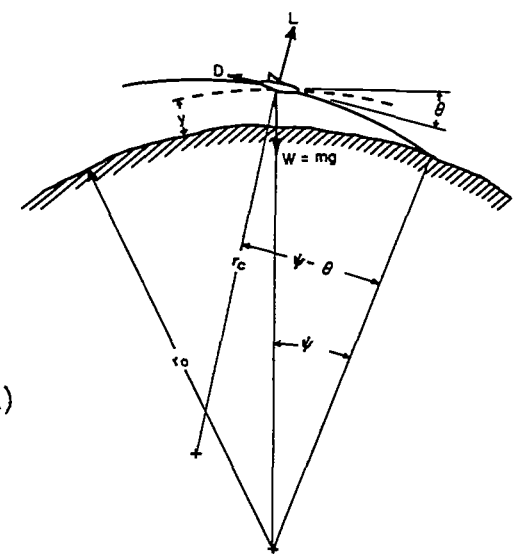

Under the assumption of small inclination angle, θ, to the horizontal (thus $\cos\theta \approx 1$, $\sin\theta \approx \theta$), constant gravity acceleration (i.e., $\frac{r}{r_o} \approx 1$) and noting that

$$\left.\begin{aligned} \frac{dV}{dt} &\equiv V\frac{dV}{ds} \equiv \frac{1}{2}\frac{dV^2}{ds} \\ \frac{1}{r_c} &= \frac{d(\psi - \theta)}{ds} \\ \frac{d\psi}{ds} &= \frac{\cos\theta}{r} \approx \frac{1}{r_o} \end{aligned}\right\} \tag{2}$$

we write equations (1) in the forms

$$\left.\begin{aligned} L &= mV^2\frac{d\theta}{ds} + mg - \frac{mV^2}{r_o} \\ D &= -mV\frac{dV}{ds} + mg\,\theta \end{aligned}\right\} \tag{3}$$

It is shown in reference 3 that at high flight speeds the inclination angle, θ, and the rate of change in this angle with flight path, $d\theta/ds$, are so small that terms involving these values may be ignored for practical purposes so that the lift is given by

$$L = mg\left(1 - \frac{V^2}{gr_o}\right) = W\left(1 - \frac{V^2}{V_s^2}\right) \tag{4}$$

where V_s is the satellite speed

$$V_s = \sqrt{gr_o} \tag{5}$$

and the drag is given by

$$D = -mV\frac{dV}{ds} \tag{6}$$

The incremental unpowered flight range may be obtained from equations (4) and (6) as

$$ds = -\frac{1}{g}\left(\frac{L}{D}\right)\left(\frac{V}{1-\frac{V^2}{V_s^2}}\right)dV$$

If at each speed the optimum lift-drag ratio is maintained, then the range in unpowered flight is a maximum and given by

$$X_u = \int_o^{X_u} ds = -\frac{1}{g}\int_{V_b}^{o}\left(\frac{L}{D}\right)_{opt}\left(\frac{V}{1-\frac{V^2}{V_s^2}}\right)dV \qquad (7)$$

Thus it is seen that this range is greatest when the average value of

$$\left(\frac{L}{D}\right)_{opt}\frac{V}{\left(1-\frac{V^2}{V_s^2}\right)}$$

over the range of speeds encompassed is a maximum. The influence of the velocity, V, in the numerator is to make the integrand large at the high end of the flight speed range. As a consequence, it is found that a major part of the flight range is covered at high flight speeds. This can be appreciated intuitively from consideration of the rate of loss of kinetic energy with flight speed.

Thus it is emphasized that for the glide vehicle one must particularly strive to obtain high lift-drag ratios at the highest Mach numbers, and that a small improvement in lift-drag ratio at high Mach numbers at the expense of a lowered lift-drag ratio at lower speeds can result in an overall improvement of range. However, as indicated in Appendix A, care must be exercised to avoid adding too much additional structural weight to attain high lift-drag ratio; otherwise the range will be decreased because of the adverse effect of reducing the ratio of initial-to-final mass.

The Optimum Lift-Drag Ratio

To study the factors which influence the optimization of the lift-drag ratio, let it be assumed that the wing leading edge is supersonic (which is the usual condition at high Mach numbers). Then the lift coefficient is given by[1]

[1]The term $2\alpha^2$ is the cross-flow term for a flat plate (see refs. 4 and 5) and is the Newtonian variation as $M\to\infty$.

$$C_L = \frac{4}{\beta}\alpha + 2\alpha^2 \tag{8}$$

Since no leading-edge suction will occur for the supersonic leading edge, the drag coefficient is given by

$$C_D = C_{D_o} + \frac{4}{\beta}\alpha^2 + 2\alpha^3 \tag{9}$$

It is convenient to express equations (8) and (9) in terms of a new variable

$$\xi = \beta\alpha \tag{10}$$

so that equations (8) and (9) become

$$\left.\begin{aligned} \beta^2 C_L &= 4\xi + 2\xi^2 \\ \beta^3 C_D &= \beta^3 C_{D_o} + 4\xi^2 + 2\xi^3 \end{aligned}\right\} \tag{11}$$

From equations (11) it can be shown that at optimum L/D

$$\beta^3 C_{D_o} = \frac{4\xi_{opt}^2 + 4\xi_{opt}^3 + \xi_{opt}^4}{1 + \xi_{opt}} \tag{12}$$

for which

$$\frac{C_{D_{opt}}}{C_{D_o}} = \frac{4 + 3\xi_{opt}}{2 + \xi_{opt}} \tag{13}$$

$$\beta^2 C_{L_{opt}} = 4\xi_{opt} + 2\xi_{opt}^2 \tag{14}$$

and

$$\frac{(L/D)_{opt}}{\beta} = \frac{2 + 2\xi_{opt}}{4\xi_{opt} + 3\xi_{opt}^2} \tag{15}$$

Table I gives $\frac{(L/D)_{opt}}{\beta}$, $\beta^2 C_{L_{opt}}$, $\frac{C_{D_{opt}}}{C_{D_o}}$, and $\beta\alpha_{opt}$(deg) in terms of the independent variable $\beta^3 C_{D_o}$. For our present purposes, it is sufficient to note that the only factor which influences the maximum lift-drag ratio at any given Mach number is the value of the drag for zero lift (if no additional drag is incurred to trim the aircraft).

Drag Reduction

The factors which, in the general case, influence the wave drag, friction drag, and base drag have been considered in the rather extensive literature. It will be the purpose herein to consider only two aspects of the minimization of drag which have not previously been given the attention that they deserve.

The first factor which must be treated concerns the compromises in design which result in increasing wave drag in order to handle satisfactorily the aerodynamic heating problem. In references 3 and 6, for example, it is noted that the excessive heating which occurs at such local "hot spots" as the leading edge of the wing and the bow of the fuselage must be given particular attention. In these references it is shown that a very practical method for reducing the convective heat input rate at such stagnation points is to round the surface since the heat input rate varies inversely as the square root of the surface radius. For the fuselage, such rounding of the bow does not incur a drag penalty, provided the rounding is not excessive and may actually result in a drag reduction for small rounding (see refs. 7 and 8). For the wing, appreciable drag penalties are incurred with even small amounts of blunting. However, this drag penalty may be made small, as was pointed out in reference 3, by sweeping the leading edge of the lifting surfaces. From Newtonian theory, the drag relief afforded by sweepback is found to depend on the cosine squared of the angle of sweep for wings of fixed span (measured normal to the plane of symmetry) and fixed leading-edge radius (measured in the plane normal to the leading edge).

$$\frac{C_{D_{le}}}{C_{D_{le_{\Lambda=0}}}} = \cos^2\Lambda \tag{16}$$

The data of reference 9 indicate that this prediction is relatively accurate. The experimental results for circular cylinders of reference 10 may be used to evaluate the drag coefficient at zero sweep for a leading edge of constant radius, σ, since at supersonic speed the foredrag of such cylinders is essentially the total drag. These results indicate that the

[redacted]

drag coefficient is nearly independent of Mach number and has the approximate value (based on cylinder frontal area) of 1.25. The drag coefficient of a swept leading edge of constant radius is therefore given by

$$C_{D_{le}} = 2.5 \frac{b\sigma}{S} \cos^2\Lambda \tag{17}$$

In addition to reducing the drag of the blunt leading edge, sweepback also reduces its heating rate. The theoretical and experimental results of reference 11 suggest that the heating rate per unit area varies approximately as[2]

$$\frac{dH}{dt} \sim \frac{\cos \Lambda}{\sqrt{\sigma}} \tag{18}$$

Therefore, for equal heating rates per unit surface area the leading-edge drag of blunt airfoils will vary as

$$C_{D_{le}} \sim \cos^4\Lambda \tag{19}$$

It is clear, then, that if large sweep is employed, the drag penalty due to rounding the leading edge can be made small.

The second factor which should be given special consideration is the frictional drag since, in general, as the Mach number is increased the relative contribution of friction to the total drag is increased. Although, as is well known, the turbulent skin-friction coefficient decreases markedly with increase in Mach number (ref. 12), it remains true that the turbulent friction usually exceeds the laminar friction and hence the possibility of maintaining laminar flow must not be overlooked. The advantages of laminar flow are twofold, improved lift-drag ratio and diminished aerodynamic heating, so that the attainment of laminar flow is especially desirable for hypervelocity vehicles. To determine whether or not long runs of laminar flow appear feasible it is necessary to determine the range of Reynolds number that will probably be covered in hypervelocity flight. To this end equation (4) can be written

$$L = W\left(1 - \frac{V^2}{V_s^2}\right) = C_L \frac{\rho V^2}{2} S \tag{4}$$

[2]As noted in reference 11, the heating rate may vary more nearly as the square of the cosine of the angle of sweep if the wall is very cool compared to stagnation temperature.

[redacted]

so that the density becomes

$$\rho = \frac{2\left(\frac{W}{S}\right)\left(1 - \frac{V^2}{V_s^2}\right)}{C_L V^2} \tag{20}$$

and hence the Reynolds number for length l becomes

$$R = \frac{\rho V l}{\mu} = \frac{2l\left(\frac{W}{S}\right)\left(1 - \frac{V^2}{V_s^2}\right)}{\mu C_L V} \tag{21}$$

From equations (20) and (21) and the values of table I, the flight altitude and Reynolds numbers per foot of length have been determined for aircraft having a constant lift-drag ratio of 5 with wing loadings of 70, 50, and 30 pounds per square foot and for aircraft having wing loadings of 50 pounds per square foot with constant lift-drag ratios of 6, 5, and 4 for speeds up to the satellite speed (25,930 ft/sec).[3] The results of these calculations are presented in figures 1 and 2. These figures show that except for a near satellite vehicle, the altitudes of interest are less than 200,000 feet. More important, it is seen that the Reynolds number, which remains nearly constant at the lower supersonic speeds, falls rapidly as the speed is increased to hypersonic values and, of course, becomes zero at satellite speed. Moreover, it should be noted that the Reynolds numbers are not large, particularly if the wing loading is low. In recent experiments (as yet unpublished) on bodies in the Ames supersonic free-flight wind tunnel, it was found that as Mach number is increased (at least up to the limiting test Mach number of 7), the attainment of long laminar-flow runs becomes easier in the sense that the laminar boundary layer is more difficult to trip with roughness. In these experiments, in fact, transition Reynolds numbers greater than 13×10^6 were found at a Mach number of 7 even for relatively rough surfaces. Since this is the

[3]It should be noted that for a given lift-drag ratio and a given Mach number the optimum lift coefficient can be determined from table I. However, for a given velocity the Mach number depends on the speed of sound and, hence, on the altitude. Thus the method employed for these calculations must be an iterative one. For a given velocity, V, the altitude of flight is assumed and the corresponding speed of sound, a, determined from reference 13. The assumed Mach number M, and, hence, β, then is used to find C_L from table I and the density ρ from equation (20). The equilibrium flight altitude corresponding to ρ is found from reference 13. The speed of sound for this altitude is used as a second approximation and this calculation procedure is repeated. This iterative process is continued until the assumed sound speed agrees with that for the altitude corresponding to the calculated ρ. The viscosity μ for the corrected altitude, and the corrected lift coefficient are then used in equation (21) to find the flight Reynolds number.

[redacted]

order of the full-scale flight Reynolds numbers indicated in figures 1 and 2 for the higher flight Mach numbers, it would not appear unreasonable for vehicles operating at the altitudes for maximum range to attain fully laminar flow.

It appears that by careful attention to the above factors a hypersonic glide airplane of low drag and therefore of usefully high lift-drag ratio could be devised. In a later section this point will be further examined by study of a particular configuration having large sweepback and otherwise designed to have low drag. First, however, attention will be turned to the problem of aerodynamic heating because, if the heating of the airplane cannot be kept within reasonable bounds, then it is not a feasible vehicle for sustained, man-carrying flight.

Heat-Transfer Reduction

The most powerful means available to the designer for controlling the heating rate of a hypersonic airplane is the selection of the flight altitude. Quantitatively, the altitude effect can be expressed in terms of Reynolds number and, for slender aircraft, can be approximated by use of the heat-transfer relations for a flat plate. Present indications, references 14 and 15, are that the modified Reynolds analogy,

$$St = \frac{0.5}{Pr^{2/3}} c_f \tag{22}$$

satisfactorily describes the heat transfer of supersonic laminar and turbulent boundary layers with small pressure gradient and wall-temperature variation, although less is known experimentally about the laminar case than the turbulent. Substitution into equation (22) of the laminar law for variation of skin-friction coefficient with Reynolds number and appropriate rearrangement yields the expression for average heat-transfer rate,

$$\frac{dH}{dt} = h(T_r - T_w) = 0.664 \frac{c_f}{c_{f_i}} Pr^{1/3} R^{1/2} \frac{k(T_r - T_w)}{l} \tag{23}$$

wherein the variables (R, k, etc.) are based on conditions just outside the boundary layer. This form of the heat-transfer equation shows direct dependence of the heat-transfer rate on the square root of Reynolds number. For turbulent boundary layer, dH/dt varies as the 4/5 root of Reynolds number. In either case, the desirability of keeping the Reynolds number low is evident.

The factors that determine the flight Reynolds number are indicated in equation (21). At this point, it is desired to focus attention on one of them - the wing loading. Certainly it is possible to design hypersonic aircraft with high wing loading or even without wings because the available dynamic pressures are very great. These vehicles, however, will be forced to fly at relatively low altitude and high Reynolds number and, consequently, will experience high heating rates. The point of view adopted herein is that the wing loading should be as low as it can be without unduly increasing the total weight (see Appendix A).

Equations (21) and (23) further suggest that low heat-transfer rate will be promoted by flight at high lift coefficient. However, the lift coefficient is already set by the requirement of efficient flight and cannot be varied arbitrarily. Also, a strongly adverse effect of high lift coefficient not apparent in equation (21) will be demonstrated in a subsequent paragraph. The effect of the factor $1 - (V^2/V_s^2)$ is to reduce the Reynolds number with increasing speed, as is shown in figure 1, and thus to counteract to some extent the strong tendency for increasing heat transfer with increasing recovery temperature which accompanies increasing Mach number.

The Reynolds numbers given by equation (21) are the free-stream length Reynolds numbers and are suitable for estimating the heat transfer for a flat plate at zero lift. In the lifting case, appreciable compression of the free-stream air occurs on the lower surface of the wing and the Reynolds number per foot at the edge of the boundary layer is affected. To examine this situation, let us first write the expression for pressure ratio on the lower surface for a wing of vanishingly small thickness,

$$\frac{p_l}{p} = \frac{\gamma}{2} M^2\left(\frac{4\alpha}{\beta} + 2\alpha^2\right) + \frac{p_u}{p} \tag{24}$$

which follows from the equation for lift coefficient. At all flight speeds considered here, the pressure acting on the wing upper surface is small compared to that on the lower surface, and at the higher Mach numbers it becomes negligible. Thus, the lower-surface pressure ratio increases with increasing Mach number, following a first power variation for small angles of attack and a quadratic variation for larger angles.

The variation of lower-surface length Reynolds number, R_l, with pressure ratio is obtained by use of the two-dimensional oblique-shock equations for $\gamma = 1.4$ and the assumption that viscosity varies as the 3/4 power of absolute temperature. This is found to be:

$$\frac{R_l}{R} = \left(\frac{6\frac{p_l}{p} + 1}{6 + \frac{p_l}{p}}\right)^{7/4}\left[1 - \frac{5\left(\frac{p_l^2}{p^2} - 1\right)}{\left(6\frac{p_l}{p} + 1\right)M^2}\right]^{1/2}\left(\frac{p_l}{p}\right)^{-3/4} \tag{25}$$

As is shown in the above equation and in figure 3(a), the Reynolds number ratio depends somewhat on the flight Mach number. More important, however, is the rather unexpected behavior of the curves which, instead of rising steadily with increasing pressure ratio, show maxima at pressure ratios between 5 and 8. This is due to the opposing actions of the density ratio and viscosity ratio. At first, density increases more rapidly than viscosity, but at the larger angles of attack, the situation is reversed. The result is relatively favorable in that the maximum increase of Reynolds number over the free-stream value is limited to 88 percent at $M = 15$ and to 88.3 percent at infinite Mach number. This has an important bearing on the heat transfer to the lower surface and also on the possibility of retaining laminar flow thereon.

In equation (23), there appears an additional variable which is strongly affected by angle of attack - the thermal conductivity of the air at the boundary-layer edge. It can be shown from available experimental values of the thermal conductivity that for usual stream static temperatures the ratio of the local (lower surface) to static thermal conductivities can be approximated by

$$\frac{k_l}{k} = \left(\frac{T_l}{T}\right)^{0.85} = \left[\frac{\frac{p_l}{p}\left(\frac{p_l}{p} + 6\right)}{6\frac{p_l}{p} + 1}\right]^{0.85} \tag{26}$$

It is convenient to combine the effects of lower-surface compression on the Reynolds number and thermal conductivity in the single expression,

$$\frac{\left(\frac{dH}{dt}\right)_l}{\left(\frac{dH}{dt}\right)_{\alpha=0}} \approx \frac{k_l}{k}\sqrt{\frac{R_l}{R}} = \left(\frac{6\frac{p_l}{p} + 1}{6 + \frac{p_l}{p}}\right)^{0.025}\left[1 - \frac{5\left(\frac{p_l^2}{p^2} - 1\right)}{\left(6\frac{p_l}{p} + 1\right)M^2}\right]^{1/4}\left(\frac{p_l}{p}\right)^{0.475} \tag{27}$$

Approximately, this equation gives the ratio of heat transfer on the lower surface for the lifting case to the heat transfer at zero lift. The first two factors on the right-hand side are weakly varying terms which remain close to 1 except at low supersonic speeds. For the higher speeds, equation (27) can be closely approximated by a simple square-root dependence on pressure ratio,

$$\frac{\left(\frac{dH}{dt}\right)_l}{\left(\frac{dH}{dt}\right)_{\alpha=0}} \approx \sqrt{\frac{p_l}{p}} \tag{28}$$

Equation (27) is plotted in figure 3(b) and shows a steady increase in heating rate with increasing pressure ratio. From this standpoint, it is clearly desirable to fly at low pressure ratios and therefore at low angles of attack.

Similar considerations applied to the upper surface of the wing indicate that an appreciable decrease in heating rate over that for flight at zero lift will be felt there. The dependence of Reynolds number on pressure ratio is now found from isentropic flow relations to be:

$$\frac{R_u}{R} = \left(\frac{p_u}{p}\right)^{\frac{7-3\gamma}{4\gamma}} \left[1 + \frac{1 - \left(\frac{p_u}{p}\right)^{\frac{\gamma-1}{\gamma}}}{\frac{\gamma-1}{2} M^2}\right]^{1/2} \tag{29}$$

This variation is plotted in figure 4(a) and shows an interestingly small dependence on Mach number. As was true on the wing lower surface, the thermal conductivity on the upper surface also varies with pressure ratio and, for the temperature range encountered there, is best represented by

$$\frac{k_u}{k} = \left(\frac{T_u}{T}\right)^{0.94} = \left(\frac{p_u}{p}\right)^{0.94\,\frac{\gamma-1}{\gamma}} \tag{30}$$

Combining equations (29) and (30) yields the expression

$$\frac{\left(\frac{dH}{dt}\right)_u}{\left(\frac{dH}{dt}\right)_{\alpha=0}} \approx \frac{k_u}{k}\sqrt{\frac{R_u}{R}} = \left(\frac{p_u}{p}\right)^{\frac{0.57\gamma - 0.065}{\gamma}} \left[1 + \frac{1 - \left(\frac{p_u}{p}\right)^{\frac{\gamma-1}{\gamma}}}{\frac{\gamma-1}{2} M^2}\right]^{1/4} \tag{31}$$

which, for $\gamma = 1.4$ becomes

$$\frac{\left(\frac{dH}{dt}\right)_u}{\left(\frac{dH}{dt}\right)_{\alpha=0}} \approx \left(\frac{p_u}{p}\right)^{0.524} \left\{1 + \frac{5\left[1 - \left(\frac{p_u}{p}\right)^{0.286}\right]}{M^2}\right\}^{1/4} \tag{32}$$

[redacted]

The second factor on the right is negligibly different from 1 at high supersonic Mach numbers, so the approximate equation, (28), holds for the upper surface as well as the lower.

Equation (32) has been plotted in figure 4(b) and indicates appreciable reductions in heating rate to the upper surface of the lifting wing over that for zero lift. Two-dimensionally, the pressure ratios needed for entry into this figure can be obtained from the Prandtl-Meyer equation for supersonic expansion at the flight Mach number and angle of attack. Comparison of figures 3 and 4 indicates the relative importance of retaining laminar flow on the wing lower surface where the heating rates are high by comparison to the upper surface.

For a given flight Mach number, then, the heating rate of the airplane will be controlled primarily by the free-stream length Reynolds number and the angle of attack. The Reynolds number will be determined by the wing loading and the ratio of flight speed to satellite speed, and the angle of attack will be defined by the lift-drag characteristic of the airplane. At some equilibrium temperature the heating rates will be balanced by heat radiation from the surface. Before the severity of the aerodynamic heating can be judged, some numerical calculations must be performed. For this purpose, consider the following example.

EXAMPLE

The Configuration

The above aerodynamic heating considerations have indicated that the hypersonic glide airplane should have a low wing loading. Moreover, at the optimum angles of attack of the airplane, the lift-drag ratio of the body will be low compared to the lift-drag ratio of the wing so that high resultant lift-drag ratio will be promoted by use of a wing that is large relative to the body. For these reasons and for reasons relating to aerodynamic stability, drag, and boundary-layer transition, the configuration chosen for the example is the one shown in figure 5.

The triangular wing with root chord equal to the fuselage length gives the maximum leading-edge sweepback consistent with the over-all length and span. Furthermore, the possibility of retaining fully laminar flow is improved, it is believed, by making the wing apex and the fuselage tip coincident (to prevent the wing shock wave from intersecting the body boundary layer). As is well known, however, the influence of wing thickness on swept wings is adverse as regards the stability of a laminar boundary layer. For this and other reasons, therefore, the configuration shown may not be optimum for purposes of retaining laminar boundary layer, and the success of this design for retaining laminar flow will have to await experimental investigation.

The symmetrical arrangement of three wings was selected rather than a more conventional planar wing with separate horizontal and vertical tails out of considerations of aerodynamic stability. The theory of Maple and Synge, reference 16, indicates that the variations in aerodynamic stability with roll position can be expected to decrease if the number of planes of symmetry is increased. The configuration of figure 5, having three planes of symmetry, should show smaller variations in stability than a conventional configuration with a single plane of symmetry. One readily apparent advantage of the symmetrical arrangement is that it provides large directional stability (to the first order of approximation equal to the longitudinal stability) without incurring large rolling moment due to sideslip. The experimental results obtained in reference 17 on this type of configuration demonstrate that such is the case, at least at low speeds. Additional stability advantages should derive from the lack of wing-tail interference and the tendency of the triangular plan form to retain a fixed center of pressure over a broad Mach number range.

Minimum Drag

The estimated minimum drag coefficients for this configuration (based on the area of the two lifting panels) is shown as a function of Mach number in figure 6. Part (a) shows the drag coefficients with fully turbulent boundary layer. The drag breakdown indicates that skin friction is a major part of the drag, especially at the higher Mach numbers. (At the lower Mach numbers the combined base drag of the body and the blunt-based wings becomes important. This could be reduced by use of boattailing but, because of primary interest in the higher end of the speed range, investigation of this aspect of the design was not pursued.) With laminar boundary layer, the skin friction is reduced appreciably, figure 6(b), and the total drag coefficients as well. Of course, the drag advantage of the laminar boundary layer depends on the Reynolds number, so it is pertinent to examine the Reynolds numbers employed in computing the results shown. Accordingly, the full-scale free-stream length Reynolds numbers are shown in figure 7 for an airplane 48 feet long. The variation shown tends to cause a diminishing difference between the laminar and turbulent drag curves with increasing Mach number, but in the speed range considered here, the laminar boundary layer retains a decided advantage with respect to both drag and heat transfer.[4] It should be noted that in computing the skin friction no consideration has been given such factors as molecular dissociation of the air, shock-wave-boundary-layer interaction, and increasing mean-free path at the higher altitudes so that these results may well be in error at the higher Mach numbers.

[4]Extension of the calculations to higher Mach numbers and the corresponding higher optimum altitudes by use of continuum flow relations led to the result that the laminar and turbulent skin friction would become equal at $M = 17.8$, $R = 1.6$ million.

[redacted]

Before proceeding, it will be of interest to show the drag of the airplane with some configuration changes to indicate the relative importance of various parts of the geometry with respect to drag. This is done in figure 8 where three items of geometry are considered: wing sweepback, nose fineness ratio, and fuselage tip radius. The base curve is the total drag coefficient of figure 6(a) with fully turbulent boundary layer. (Use of the laminar drag curve, of course, would make the drag increments somewhat larger percentagewise.) In part (a), the change in total drag due to changing the sweepback of the leading edge is shown for leading edges of fixed radius and fixed span normal to the body axis.[5] With the unswept wing, the drag of the blunt leading edge is prohibitively high, and the penalty at 45° sweepback is still severe. It is evident that the wing sweepback is a paramount consideration in minimizing the drag. In part (b), the effect of nose fineness ratio is considered for tangent ogival noses in fuselages of the same total length. The fineness-ratio-3 nose, while adding to the useful volume of the fuselage, is also seen to add appreciably to the drag. Finally, in part (c), the effect of fuselage tip bluntness is shown. The 5-percent-blunt tip selected causes essentially no drag penalty, but significant penalties arise when the tip bluntness approaches 25 percent.

Lift-Drag Ratio

The optimum lift-drag ratios corresponding to the minimum drag coefficients of figure 6 are given in figure 9. These are computed from the lift and drag equations, (8) and (9), by use of table I. No allowance is included for the trim lift or trim drag. The values obtained are relatively high for this speed range and are comparable to experimental values at Mach numbers near 2. Very recently, lift-drag ratios of this magnitude have been realized experimentally in tests of highly swept triangular wings at a Mach number of 6.9 (ref. 18). The computed lift-drag ratios are relatively constant over the Mach number range and are from 13 to 24 percent higher with laminar boundary layer than with turbulent. A typical variation of L/D with angle of attack is shown in figure 10 for a Mach number of 8. The optimum angles of attack for the entire Mach number range are nearly the same as those shown, between 5° and 6° with laminar boundary layer and near 7° with turbulent boundary layer. The lift coefficients, on the other hand, decrease steadily with increasing flight speed (fig. 11). This, of course, is due to the steady decrease in initial lift-curve slope with rising Mach number.

[5]It is considered that the wing area remains constant so that skin friction does not change. The wing pressure drag other than that acting at the leading edge is also assumed constant so that the drag changes shown are due solely to variations in pressure drag of the leading edge.

Aerodynamic Heating of "Hot Spots"

It remains to consider the aerodynamic heating of this airplane. As an example of severe local heating, the heating of the wing leading edge will be discussed herein. Other locations which will not be analyzed but which will encounter similarly severe heating include the fuselage tip and the transition region should boundary-layer transition occur.

The theory and experiment of reference 11 and unpublished tests in the Langley 11-inch hypersonic wind tunnel on the heating rates of swept and unswept two-dimensional circular cylinders indicate that the average heating rates at the wing leading edge will depend on leading-edge radius, sweepback angle, and Reynolds number per foot in accordance with the following approximate equation

$$\frac{dH}{dt} = C \cos \Lambda \sqrt{\frac{\rho V}{\mu}}\, k(T_r - T_w)\sigma^{-1/2} \qquad (33)$$

The constant C is found to have the value 1.94 in the Langley tests at a Mach number of 6.9, Reynolds number of 135,000, and wall to free-stream temperature ratio of 6.3. The tests of reference 11, in the Ames hypersonic gun tunnel at $M = 9.8$, $R = 315$, and $T_w/T_o = 4.9$, indicate that if the entire measured heat transfer is ascribed to the forward half of the cylinder, the constant C has the value of 2.02. It may be found ultimately that this constant will depend on Mach number and wall-temperature ratio but, for the present calculation, the value 2.0 will be assumed to apply universally.

With the aid of equation (33) the effects of sweepback[6] and leading-edge radius on leading-edge heating rate have been examined for a flight Mach number of 7 at optimum altitude, 120,000 feet. In figure 12, heating rates for several configurations are plotted as a function of leading-edge temperature and vanish for all configurations at the recovery temperature for this Mach number and altitude, 4400° F. The heat emission rate due to radiation from the leading edge is also indicated for two values of emissivity, 0.6 and 0.9. The first case considered is a sharp unswept leading edge with a radius of 0.015 inch. The heating rate is found to be very great and radiation equilibrium occurs at a leading-edge temperature of about 3500° F. Blunting the unswept leading edge to 0.75-inch radius reduces the equilibrium temperature to about 2500° F but incurs the large drag penalty shown in figure 8(a). By use of sweepback, both the

[6]For $\Lambda > 60°$, the $\cos \Lambda$ variation underestimates the heat-transfer rate since the cosine goes to zero at $\Lambda = 90°$, whereas the heating rate does not. Therefore, the heating rates for $\Lambda = 74°$ were calculated using experimental data which show the heating rate reduced to 35 percent of the unswept value.

drag and the heating rate are reduced as shown in figures 8(a) and 12 for 45° and 74° of sweep. (At 74° sweepback, the equilibrium temperature reduces to the order of 2000° F.) At best, the leading-edge heating is severe and it would seem desirable to isolate the leading edge both thermally and structurally, insofar as possible.

The next thing considered is the effect of flight Mach number on the equilibrium temperature of the leading edge of the airplane with 74° sweepback and a leading-edge radius of 0.75 inch. Of course, the radiation equilibrium temperature of the leading edge is increased by increasing the Mach number, principally through the action of the increased recovery temperature, but is also affected favorably by the reduced flight Reynolds number and unfavorably by the increased free-stream air conductivity in the hotter air at high altitudes.[7] The resulting variation of equilibrium leading-edge temperature with Mach number is shown in figure 13. Some very high temperatures are reached, approaching but still below the melting temperatures of a few metals and refractory materials. The possibility of significantly reducing the leading-edge temperatures below those shown by any means short of incorporating a cooling system are not felt to be extremely promising. Further increasing the sweepback will help some but, at 74°, the rate of fall of heating rate with sweepback has passed its maximum. Decreases in wing loading may not be feasible since the value of 30 pounds per square foot is already considered low. Increasing the leading-edge radius will reduce the temperature somewhat but no significant reduction could be realized without an appreciable penalty in increased drag. Hence, leading-edge temperatures of the order of those shown may have to be accepted unless cooling by means other than radiation is employed.

Aerodynamic Heating of the Average Surface

The average heat transfer experienced by the wings will be computed from equation (23) for laminar flow and its counterpart for turbulent boundary layers.[8] The effects of lifting flight on Reynolds number and

[7]Because of the opposing effects of increasing altitude on Reynolds number and free-stream thermal conductivity, the possibility was investigated that the heating rates would be less if the flight altitude were held fixed at the top of the isothermal altitude range, 105,000 feet, where the free-stream temperature is only 390° Rankine. The heating there proved to be more severe than at the optimum flight altitude because Reynolds numbers as great as 71 million were incurred.

[8]The average skin friction and heat transfer of the triangular wings are analyzed by assuming that the streamlines are everywhere parallel to the root chord. The chordwise length Reynolds number is a function of spanwise position. Integration of the skin friction on this basis yields the result that, for laminar flow, the average skin-friction coefficient and heat-transfer rate are 4/3 of that for a flat plate with the Reynolds number of the root chord. For a turbulent boundary layer the factor is 10/9.

thermal conductivity, shown in figures 3 and 4, will be applied, as will some additional effects of lifting flight, on the skin-friction ratio, c_f/c_{f_i}, recovery temperature, and the Prandtl number at the boundary-layer edge. Of the latter three, only the first is found to be significant. The computations lead to the average heating rates shown in figure 14 for the wing surfaces at radiation equilibrium temperature. The heat-transfer rates are an order of magnitude below those developed at the leading edge at the same Mach number. The heating rates of the lower surface are up to 18 times greater than on the upper surface and are appreciably higher when the boundary layer is turbulent. The low heating rate encountered on the wing upper surface is due to the fact that the lowering of Reynolds number and thermal conductivity in the expanded stream above the wing tends to reduce the heating rate faster than increasing Mach number acts to increase it.

The average temperatures of the wing at radiation equilibrium are shown in figure 15. When it is considered that the recovery temperatures range up to 14,500° F at a Mach number of 12 (no dissociation considered), these equilibrium temperatures are quite low. With laminar boundary layer, the average temperature of the lower surface remains below 1400° F. Under these circumstances, man-carrying flight at these speeds would not appear beyond reason.

CONCLUDING REMARKS

Some design considerations relating to an airplane for unpowered gliding flight through the atmosphere at hypersonic speeds have been examined. It is noted that a major portion of the flight range will be covered at the higher speeds and that attaining a high lift-drag ratio at these speeds is important to achieving good range. Correspondingly, the lift-drag ratio at the lower speeds is relatively of less importance. For the attainment of good lift-drag ratio at high Mach numbers, careful attention to reduction of the minimum drag is required. The wings employed should be highly swept, so that the leading-edge bluntness required to reduce aerodynamic heating will not unduly raise the drag. Attention is also called to the relatively low flight Reynolds numbers to be expected and the consequent possibility of retaining a fully laminar boundary layer, which is doubly desirable because it reduces the airplane drag and the aerodynamic heating. The influence of flight altitude on the severity of the aerodynamic heating is examined and it is concluded that with low wing loading flight can occur at high altitude and, consequently, with low aerodynamic heating rates.

These considerations are applied to the study of an example airframe. It is found that reasonably high lift-drag ratios, in the order of 5 to 6, can be achieved by use of extreme sweepback and large lifting area. The heating of the wing leading edge in equilibrium flight at optimum altitude is found to be greatly relieved by the highly swept plan form chosen.

[redacted]

Nevertheless, radiation equilibrium temperatures up to 3100° F occur at the highest Mach number, 12, considered. It appears that the wing leading-edge heating constitutes one of the serious problems in the design of this type aircraft and that structural and thermal isolation of the leading edge is to be desired. The average heating of the airplane wing is then considered and found to be an order of magnitude less severe than at the leading edge. In fact, the radiation equilibrium temperature of the wing lower surface remains below 1400° F with laminar boundary layer at the highest Mach number, in the presence of a recovery temperature of 14,500°. The occurrence of relatively low equilibrium temperatures over most of the surface of the airplane is considered an encouraging indication with respect to the feasibility of this type of vehicle.

Ames Aeronautical Laboratory
National Advisory Committee for Aeronautics
Moffett Field, Calif., May 26, 1955

APPENDIX A

RANGE OF FLIGHT

In the powered phase of flight, it would appear that maximum impulse to the vehicle would be obtained by climbing and accelerating the vehicle in much the same manner as the vehicle descends and decelerates in the unpowered glide phase. In this way the useful thrust, which is the rocket thrust less the drag, will be nearly maximum. Again the assumptions of small θ and $\frac{d\theta}{ds}$ will be used. These assumptions are, of course, grossly violated if flight starts at zero velocity, but if one considers that this boost phase initiates from slight supersonic speeds (i.e., from an air-launching airplane or after a primary boost from earth), then the assumptions are valid. In any event, the flight range will not be materially affected by the course of events during this primary boost.

The equations (4) and (6) become, for the powered phase of flight

$$L = mg\left(1 - \frac{V^2}{V_s{}^2}\right) \tag{A1}$$

$$D = T - m\frac{dV}{dt} = T - \frac{1}{2}m\frac{dV^2}{ds} \tag{A2}$$

For simplicity, let us assume that

$$T = KL = Kmg\left(1 - \frac{V^2}{V_s{}^2}\right) \tag{A3}$$

where K is a constant. Then, combining these equations

$$\left(\frac{L}{D}\right)Kmg\left[1 - \left(\frac{V}{V_s}\right)^2\right] - \frac{1}{2}\left(\frac{L}{D}\right)mV_s{}^2\frac{d\left(\frac{V}{V_s}\right)^2}{ds} = mg\left[1 - \left(\frac{V}{V_s}\right)^2\right]$$

so that

$$\left[K\left(\frac{L}{D}\right) - 1\right]ds = \left(\frac{L}{D}\right)\left(\frac{V_s^2}{2g}\right)\frac{d\left(\frac{V}{V_s}\right)^2}{\left[1 - \left(\frac{V}{V_s}\right)^2\right]} \tag{A4}$$

which yields on integration from 0 to s (corresponding to from V = 0 to V = V_b) for constant $\frac{L}{D}$

$$s = \frac{-\frac{L}{D}}{K\left(\frac{L}{D}\right) - 1}\left(\frac{V_s^2}{2g}\right)\ln\left[1 - \left(\frac{V_b}{V_s}\right)^2\right] \tag{A5}$$

Hence, the range of powered flight is

$$X_p = -\left[\frac{\frac{L}{D}}{K\left(\frac{L}{D}\right) - 1}\right]\left(\frac{V_s^2}{2g}\right)\ln\left[1 - \left(\frac{V_b}{V_s}\right)^2\right] \tag{A6}$$

The maximum acceleration for a man-carrying vehicle must, of course, be limited. If a man can withstand as a maximum (which occurs at V = 0)

$$ng = \frac{T - D}{m} = \left(K - \frac{1}{L/D}\right)g$$

then

$$K = n + \frac{1}{L/D} \tag{A7}$$

and thus equation (A6) becomes

$$X_p = -\frac{V_s^2}{2gn}\ln\left[1 - \left(\frac{V_b}{V_s}\right)^2\right] \tag{A8}$$

At constant $\frac{L}{D}$ the unpowered flight range is from equation (7)

$$X_u = -\frac{L}{D}\left(\frac{V_s^2}{2g}\right)\ln\left[1 - \left(\frac{V_b}{V_s}\right)^2\right] \tag{A9}$$

so that the total range is

$$X = -\frac{V_s^2}{2g}\left(\frac{L}{D} + \frac{1}{n}\right)\ln\left[1 - \left(\frac{V_b}{V_s}\right)^2\right] \tag{A10}$$

and the fraction of the flight range which is powered is

$$\frac{X_p}{X} = \frac{1}{n\left(\frac{L}{D}\right) + 1} \tag{A11}$$

from which it is seen that for reasonable values of n (say 3) and $\frac{L}{D}$ (say 5), the powered range is but a small part of the total.

From the fact that

$$T = Kmg\left[1 - \left(\frac{V}{V_s}\right)^2\right] = -Ig\frac{dm}{dt} = -IgV_s\left(\frac{V}{V_s}\right)\frac{dm}{ds}$$

then using ds from equation (A4) it can be found that

$$V_b = Ig\left[\frac{n\left(\frac{L}{D}\right)}{n\left(\frac{L}{D}\right) + 1}\right]\ln\left(\frac{m_o}{m_b}\right) \tag{A12}$$

from which it is readily apparent that improvement in burnout velocity is only slightly influenced by the lift-drag ratio if the lift-drag ratio is already high, and care must be exercised, if high flight speed is desired, to prevent extra structural weight from decreasing V_b by reduction of the mass ratio.

Although the burnout velocity is not strongly influenced by lift-drag ratio, the flight range is, as noted from equation (7). Thus, both lift-drag ratio and mass ratio are important for range. In fact it can be shown that the range in nondimensional form (from eqs. (A12) and (A10)) becomes

[redacted]

$$\frac{2gnX}{V_s^2} = -\left[n\left(\frac{L}{D}\right) + 1\right]\ln\left(1 - \left\{\frac{Ign\left(\frac{L}{D}\right)}{V_s\left[n\left(\frac{L}{D}\right) + 1\right]}\right\}^2 \ln^2 \frac{m_o}{m_b}\right) \qquad (A13)$$

The relative influence of mass ratio and lift-drag ratio can be determined from figure 16 which gives values of nX from equation (A13) for an arbitrary specific impulse of 225 seconds. This chart should not be used when ranges corresponding to velocities close to satellite speed are considered, by virtue of the overly conservative assumption of equation (A3) and, in any event, is of value only for comparative purposes since the assumption regarding the decrease of thrust with mass is unrealistic for most practical cases.

Equation (A10) can be expressed in a form analogous to equation (A13) as

$$\frac{2gnX}{V_s^2} = -\left[n\left(\frac{L}{D}\right) + 1\right]\ln\left[1 - \left(\frac{V_b}{V_s}\right)^2\right] \qquad (A14)$$

The values of nX from equation (A14) have been calculated and are given in figure 17 as a function of the ratio $n\left(\frac{L}{D}\right)$ and the burnout velocity, V_b. The limitations for the values given in this figure are the same as those for figure 16.

REFERENCES

1. Sänger, Eugen: Raketen-flugtechnik. R. Oldenbourg, (Berlin) 1933.

2. Sänger, E., and Bredt, I.: A Rocket Drive for Long Range Bombers. BuAer, Navy Dept., CGD-32, 1947.

3. Eggers, Alfred J., Jr., Allen, H. Julian, and Neice, Stanford E.: A Comparative Analysis of the Performance of Long-Range Hypervelocity Vehicles. NACA RM A54L10, 1954.

4. Ivey, H. Reese, and Cline, Charles W.: Effect of Heat-Capacity Lag on the Flow Through Oblique Shock Waves. NACA TN 2196, 1950.

5. Flax, A. H., and Laurence, H. R.: The Aerodynamics of Low-Aspect-Ratio Wing and Wing-Body Combinations. CAL 37, Cornell Aero. Lab., Inc., Buffalo, New York, 1951.

6. Allen, H. Julian, and Eggers, A. J., Jr.: A Study of the Motion and Aerodynamic Heating of Missiles Entering the Earth's Atmosphere at High Supersonic Speeds. NACA RM A53D28, 1953.

7. Eggers, A. J., Jr., Dennis, David H., and Resnikoff, Meyer M.: Bodies of Revolution for Minimum Drag at High Supersonic Airspeeds. NACA RM A51K27, 1952.

8. Seiff, Alvin, Sandahl, Carl A., Chapman, Dean R., Perkins, Edward W., and Gowen, Forrest E.: Aerodynamic Characteristics of Bodies at Supersonic Speeds. A Collection of Three Papers. NACA RM A51J25, 1951.

9. Penland, Jim A.: Aerodynamic Characteristics of Circular Cylinders at Mach Number 6.86 and Angles of Attack up to 90°. NACA RM L54A14, 1954.

10. Gowen, Forrest E., and Perkins, Edward W.: Drag of Circular Cylinders for a Wide Range of Reynolds Numbers and Mach Numbers. NACA TN 2960, 1953. (Formerly NACA RM A52C20)

11. Eggers, A. J., Jr., Hansen, C. Frederick, and Cunningham, Bernard E.: The Effect of Yaw on Heat Transfer to a Cylindrical Stagnation Region in Hypersonic Flow. NACA RM A55E02, 1955.

12. Sommer, Simon C., and Short, Barbara J.: Free-Flight Measurements of Turbulent-Boundary-Layer Skin Friction in the Presence of Severe Aerodynamic Heating at Mach Numbers From 2.8 to 7.0. NACA TN 3391, 1955.

[redacted]

13. Warfield, Calvin N.: Tentative Tables for the Properties of the Upper Atmosphere. NACA TN 1200, 1947.

14. Van Driest, E. R.: The Laminar Boundary Layer With Variable Fluid Properties. Heat Transfer and Fluid Mechanics Institute, Univ. of Calif., June 30, July 1, 2, 1954, pp. 127-141.

15. Seiff, Alvin: Examination of the Existing Data on the Heat Transfer of Turbulent Boundary Layers at Supersonic Speeds From the Point of View of Reynolds Analogy. NACA TN 3284, 1954.

16. Maple, C. G., and Synge, J. L.: Aerodynamic Symmetry of Projectiles. Quart. Appl. Math., vol. VI, no. 4, Jan. 1949, pp. 345-366.

17. Delany, Noel K.: Exploratory Investigation of the Low-Speed Static Stability of a Configuration Employing Three Identical Triangular Wing Panels and a Body of Equal Length. NACA RM A55C28, 1955.

18. Bertram, Mitchel H., and McCauley, William D.: An Investigation of the Aerodynamic Characteristics of Thin Delta Wings With a Diamond Section at Mach Number of 6.9. NACA RM L55B14, 1955.

TABLE I.- LIFT-DRAG RATIOS FOR WINGS WITH SUPERSONIC LEADING EDGES

$\beta^3 C_{D_o}$	$\beta^2 C_{L_{opt}}$	$\frac{C_{D_{opt}}}{C_{D_o}}$	$\beta\alpha_{opt}$, deg	$\frac{\left(\frac{L}{D}\right)_{opt}}{\beta}$	$\beta^3 C_{D_o}$	$\beta^2 C_{L_{opt}}$	$\frac{C_{D_{opt}}}{C_{D_o}}$	$\beta\alpha_{opt}$, deg	$\frac{\left(\frac{L}{D}\right)_{opt}}{\beta}$
0	0	2.000	0	---	2.0	3.70	2.256	39.4	0.820
.005	.145	2.017	2.01	14.4	2.5	4.21	2.276	43.7	.740
.01	.206	2.024	2.86	10.2	3.0	4.68	2.293	47.5	.680
.02	.293	2.034	4.01	7.20	3.5	5.14	2.308	51.1	.636
.03	.360	2.041	4.93	5.88	4.0	5.59	2.321	54.3	.602
.04	.416	2.047	5.67	5.08	4.5	6.01	2.333	57.9	.572
.05	.467	2.053	6.36	4.55	5	6.41	2.344	60.2	.547
.06	.515	2.057	6.99	4.17	6	7.18	2.363	65.3	.506
.07	.560	2.062	7.56	3.88	7	7.89	2.379	69.9	.474
.08	.603	2.066	8.08	3.65	8	8.58	2.394	74.5	.448
.09	.641	2.070	8.54	3.44	9	9.23	2.407	78.5	.426
.10	.679	2.073	9.00	3.28	10	9.86	2.418	82.5	.408
.12	.750	2.079	9.91	3.01	11	10.6	2.428	86.0	.396
.14	.813	2.085	10.7	2.79	12	11.1	2.438	89.4	.379
.16	.873	2.091	11.4	2.61	14	12.2	2.455	95.7	.356
.18	.932	2.096	12.1	2.47	16	13.3	2.469	101	.337
.20	.989	2.100	12.7	2.35	18	14.3	2.482	107	.321
.25	1.12	2.110	14.2	2.12	20	15.3	2.493	112	.308
.30	1.24	2.120	15.6	1.95	25	17.7	2.517	123	.281
.35	1.35	2.128	16.8	1.81	30	19.9	2.536	132	.262
.40	1.45	2.135	17.9	1.70	35	22.0	2.552	141	.246
.45	1.55	2.142	19.0	1.61	40	24.0	2.566	150	.234
.50	1.64	2.149	20.1	1.53	45	25.9	2.578	157	.224
.60	1.82	2.160	21.9	1.41	50	27.8	2.588	164	.215
.70	1.99	2.171	23.7	1.31	55	29.6	2.597	170	.207
.80	2.15	2.181	25.2	1.23	60	31.2	2.606	176	.200
.90	2.30	2.189	26.7	1.17	70	34.6	2.621	188	.189
1.00	2.44	2.197	28.1	1.12	80	37.9	2.634	198	.180
1.2	2.72	2.211	30.5	1.03	90	40.8	2.645	208	.171
1.4	2.98	2.224	33.1	.958	100	43.7	2.654	217	.165
1.6	3.23	2.236	35.4	.902	110	46.5	2.662	225	.159
1.8	3.47	2.246	37.5	.859	120	49.3	2.670	233	.154
					130	52.0	2.677	240	.149

[redacted]

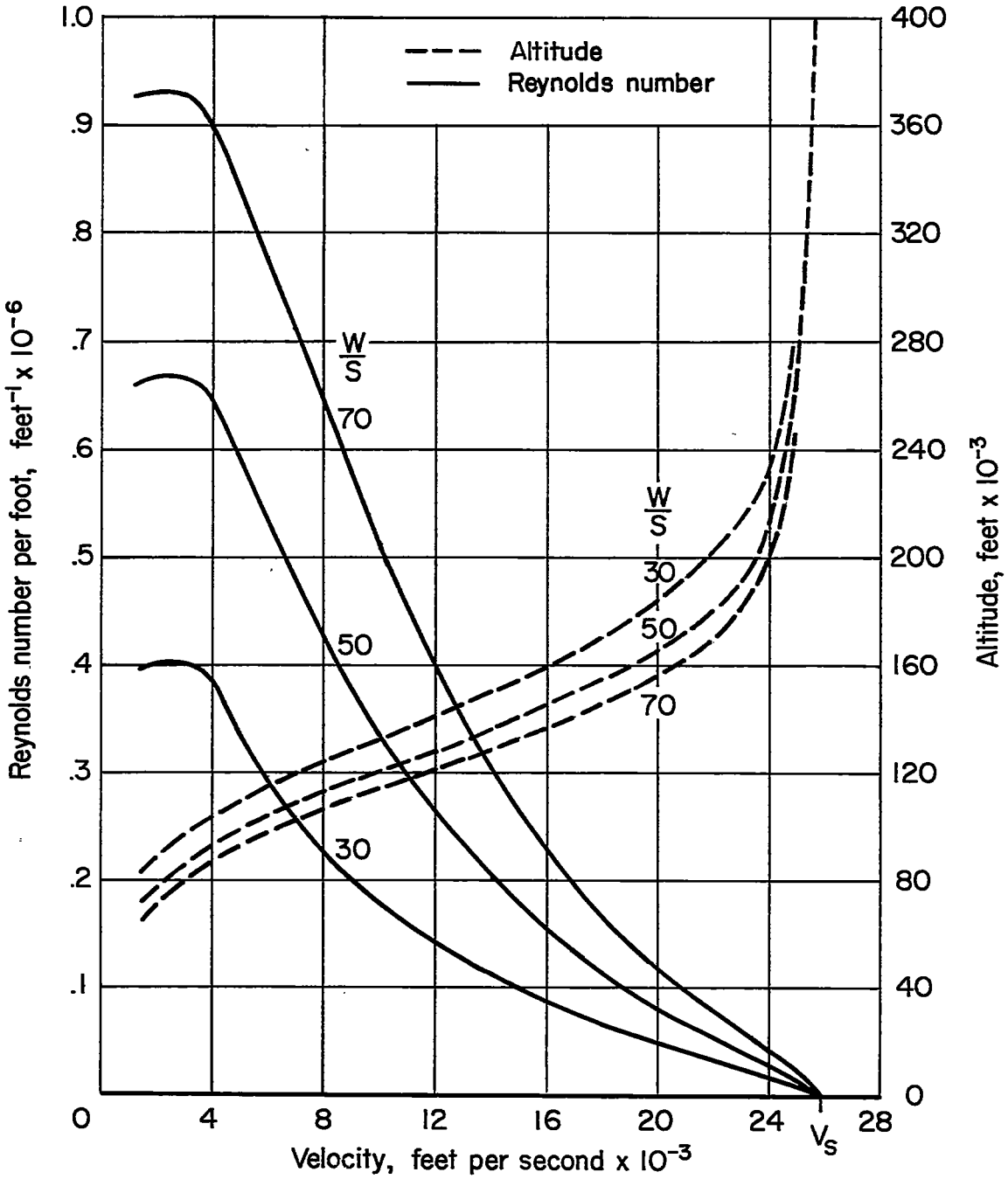

Figure 1. - Effect of wing loading and speed on flight altitude and Reynolds number for a glide vehicle with lift-drag ratio of 5.

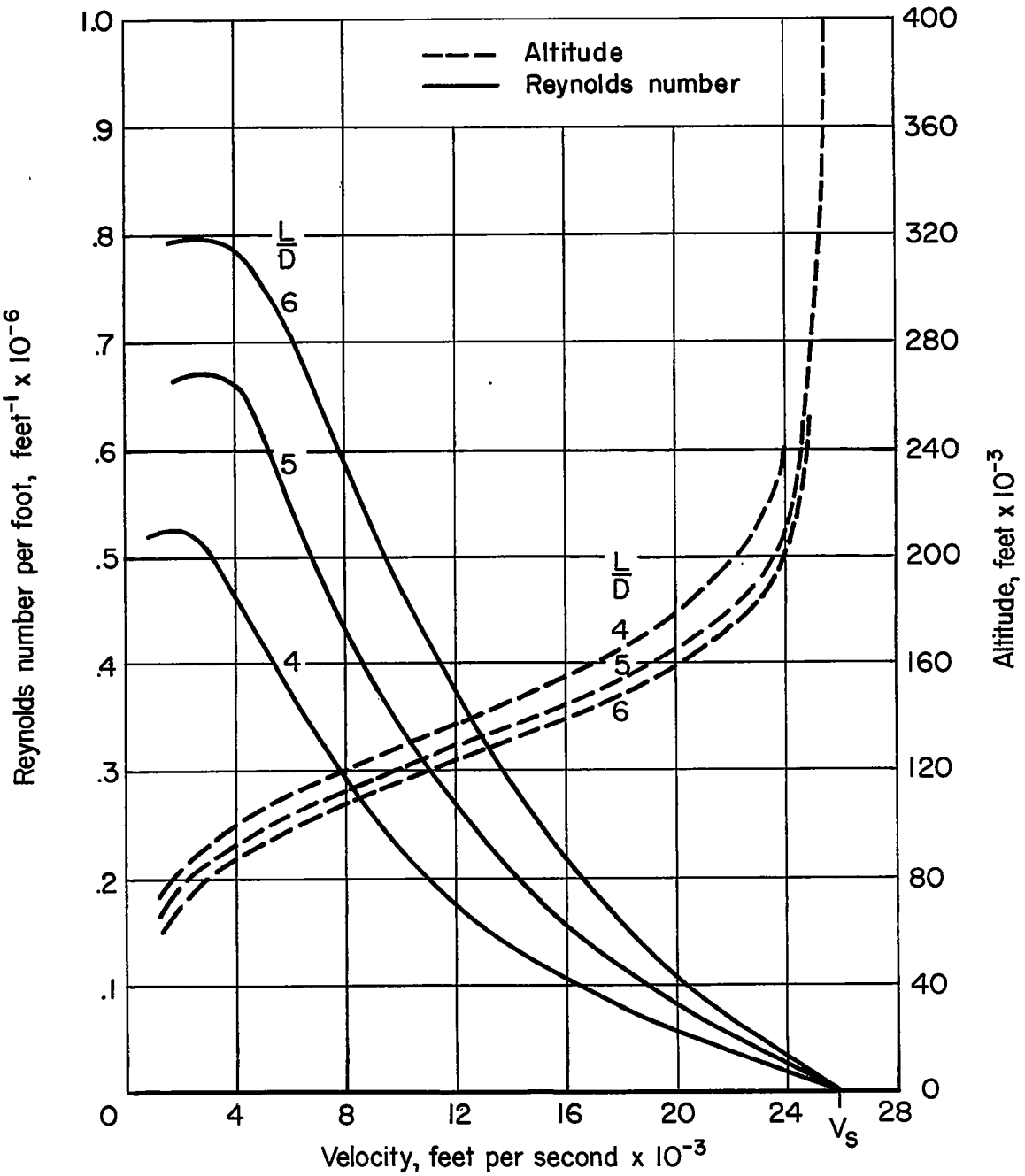

Figure 2. - Effect of lift-drag ratio and speed on flight altitude and Reynolds number for a glide vehicle with a wing loading of 50 pounds per square foot.

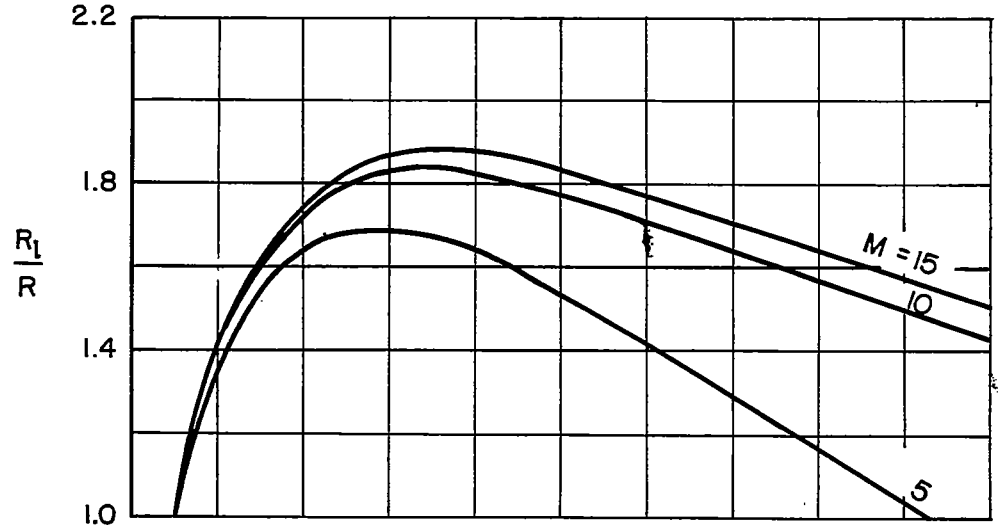

(a) Reynolds number

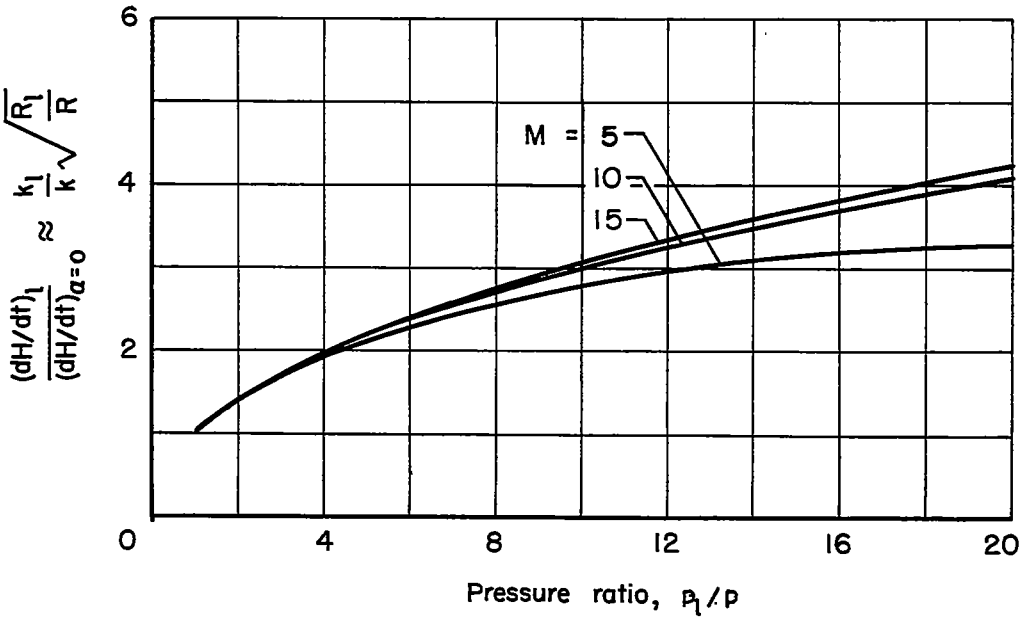

(b) Heating rate

Figure 3. - Effect of wing lower-surface pressure ratio on the Reynolds number and heating rate with laminar boundary layer.

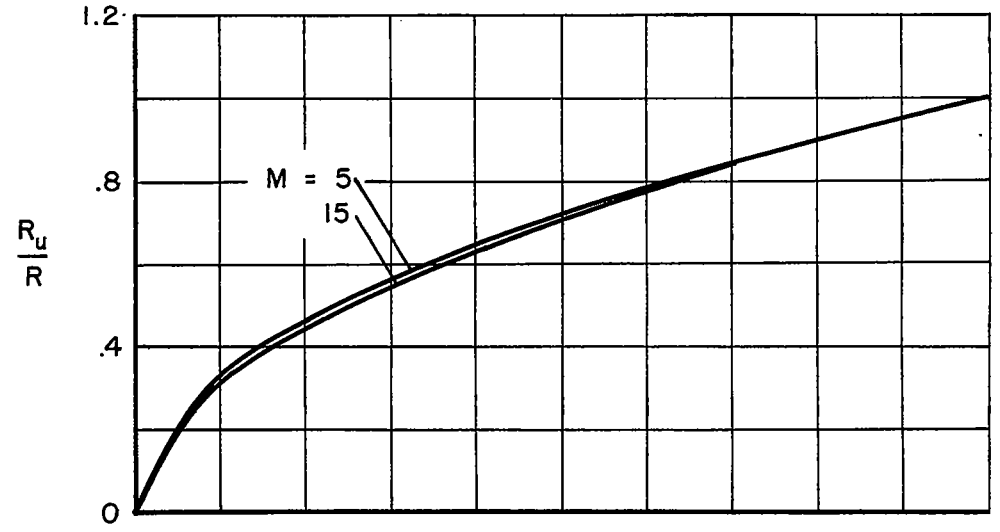

(a) Reynolds number

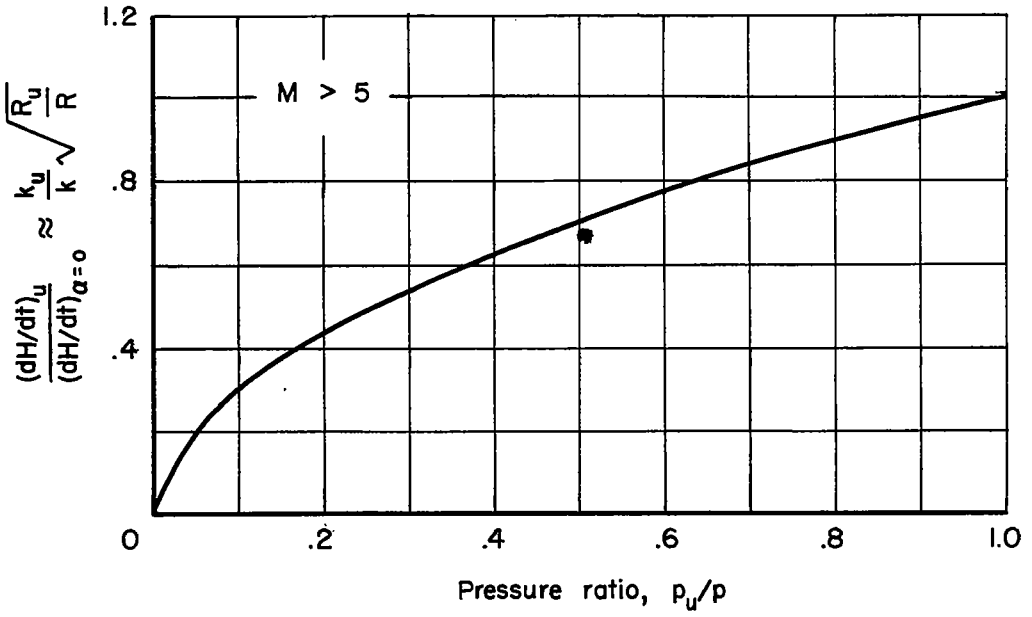

(b) Heating rate

Figure 4. - Effect of wing upper-surface pressure ratio on the Reynolds number and heating rate with laminar boundary layer.

Body fineness ratio — 9.5

Nose — tangent ogive of fineness ratio 5, with tip blunted to spherical radius of 5% of maximum body radius

b/d = 5.5

Wing thickness ratio — 2% at root

Cylindrical leading edge of constant radius = .066 maximum wing thickness

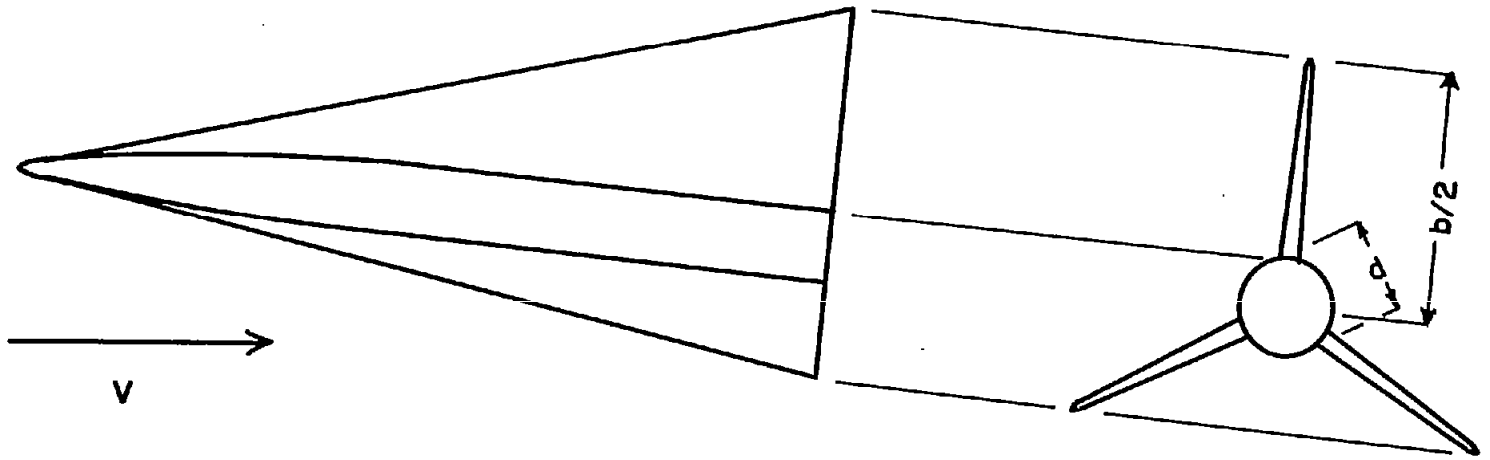

Figure 5.- Configuration used in example.

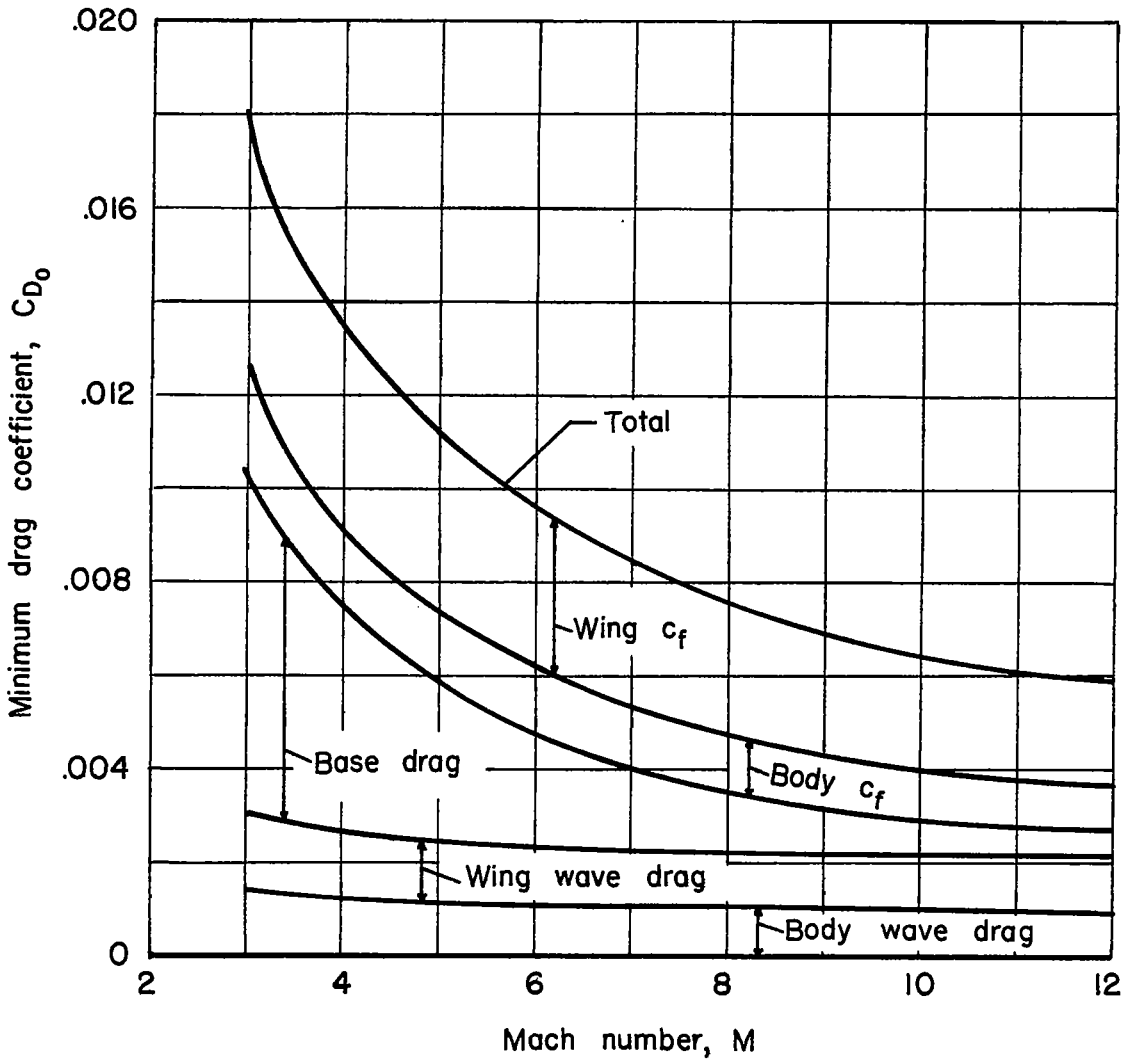

(a) Turbulent boundary layer.

Figure 6. - Estimated minimum drag coefficients of example airplane.

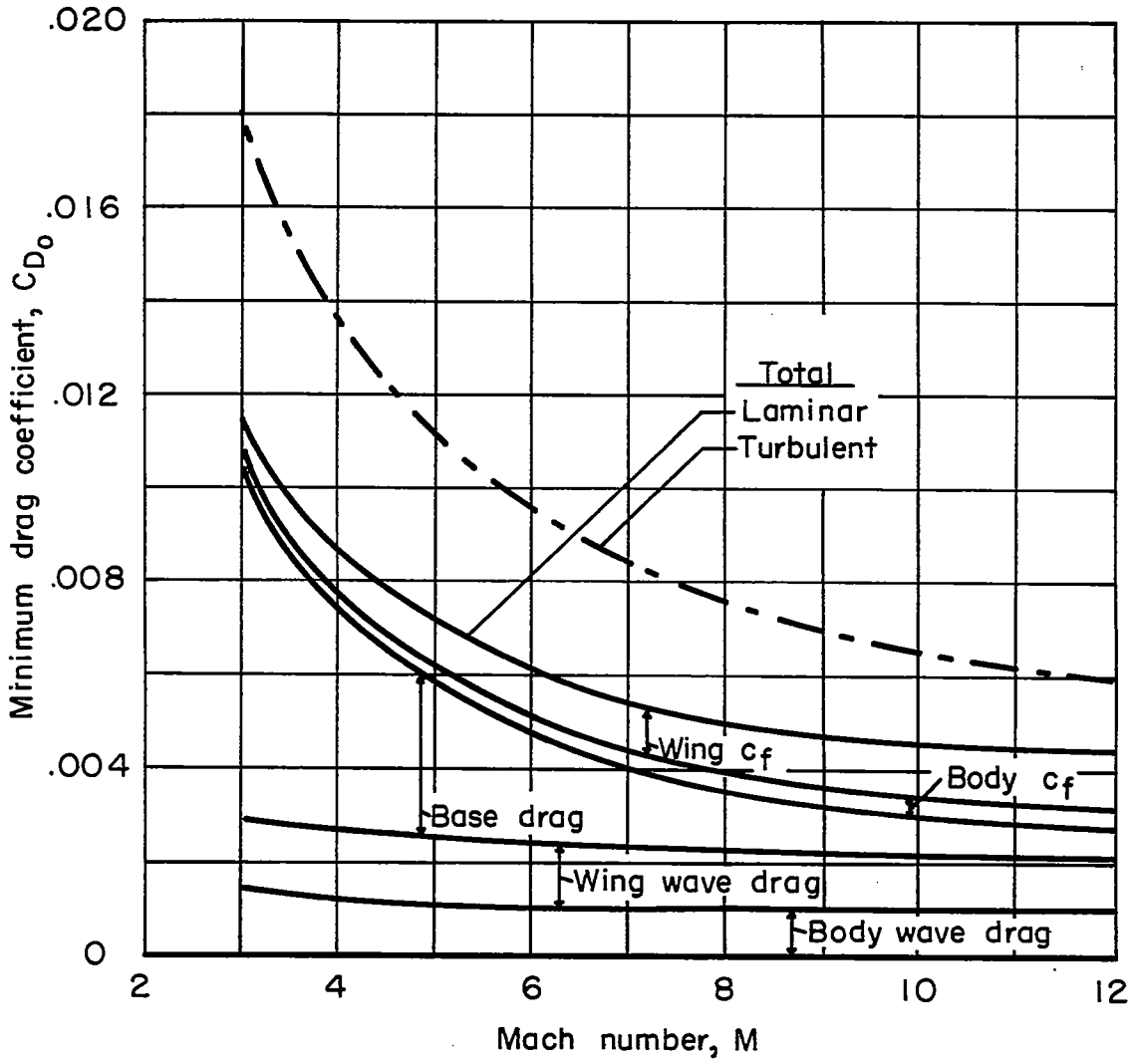

(b) Laminar boundary layer

Figure 6.- Concluded.

[redacted]

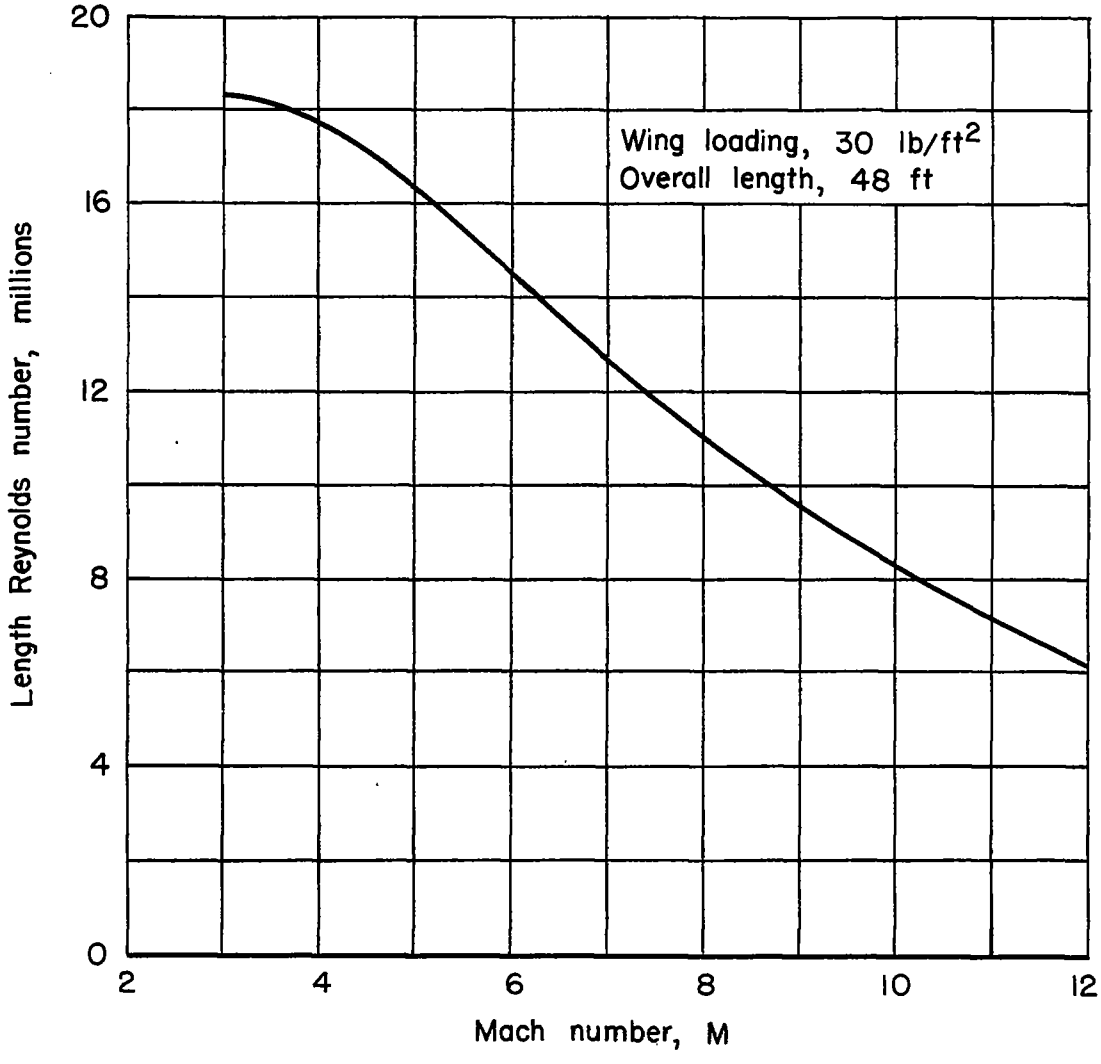

Figure 7. - Length Reynolds numbers for optimum flight of the example airplane.

[redacted]

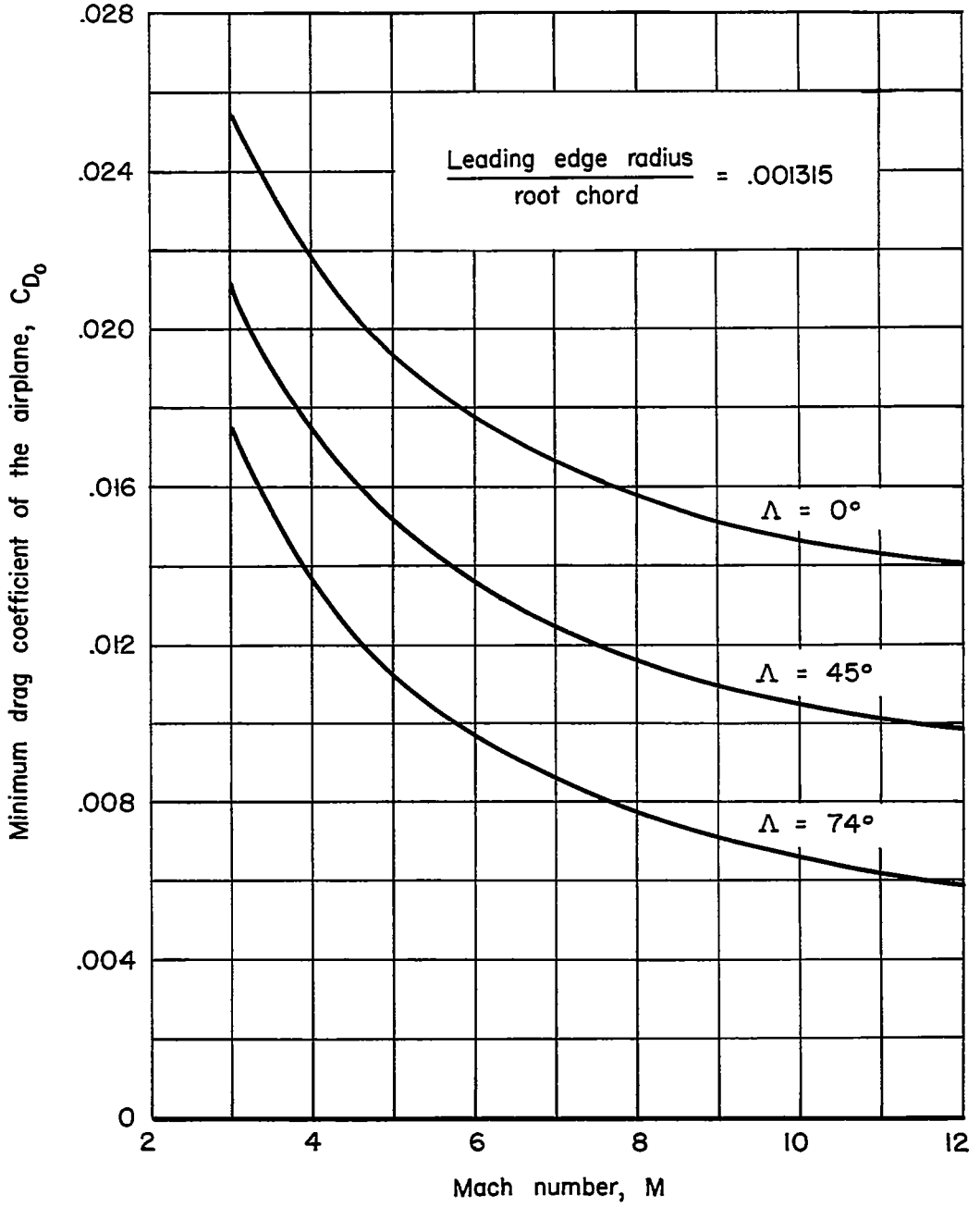

(a) Effect of sweepback (fixed span).

Figure 8. - Some effects of configuration geometry on the minimum drag with turbulent boundary layer.

[redacted]

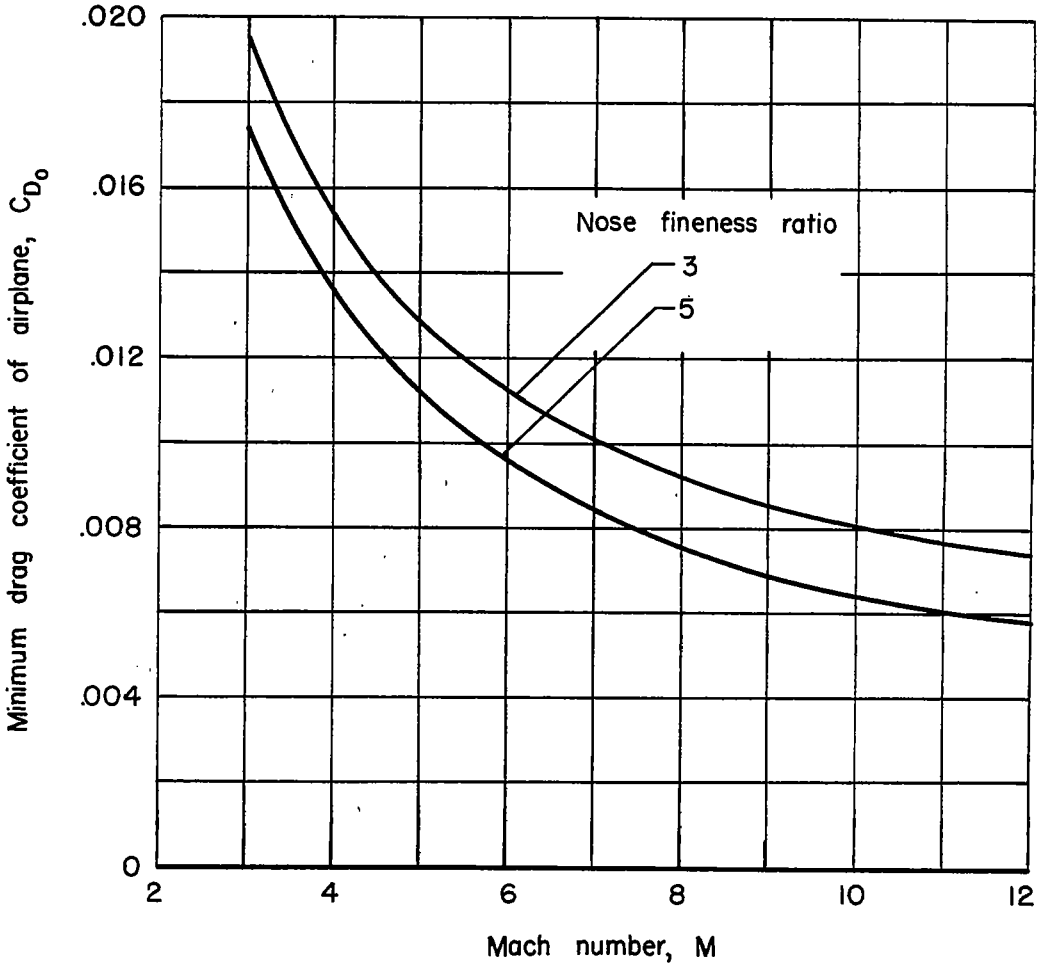

(b) Effect of nose fineness ratio.

Figure 8. - Continued.

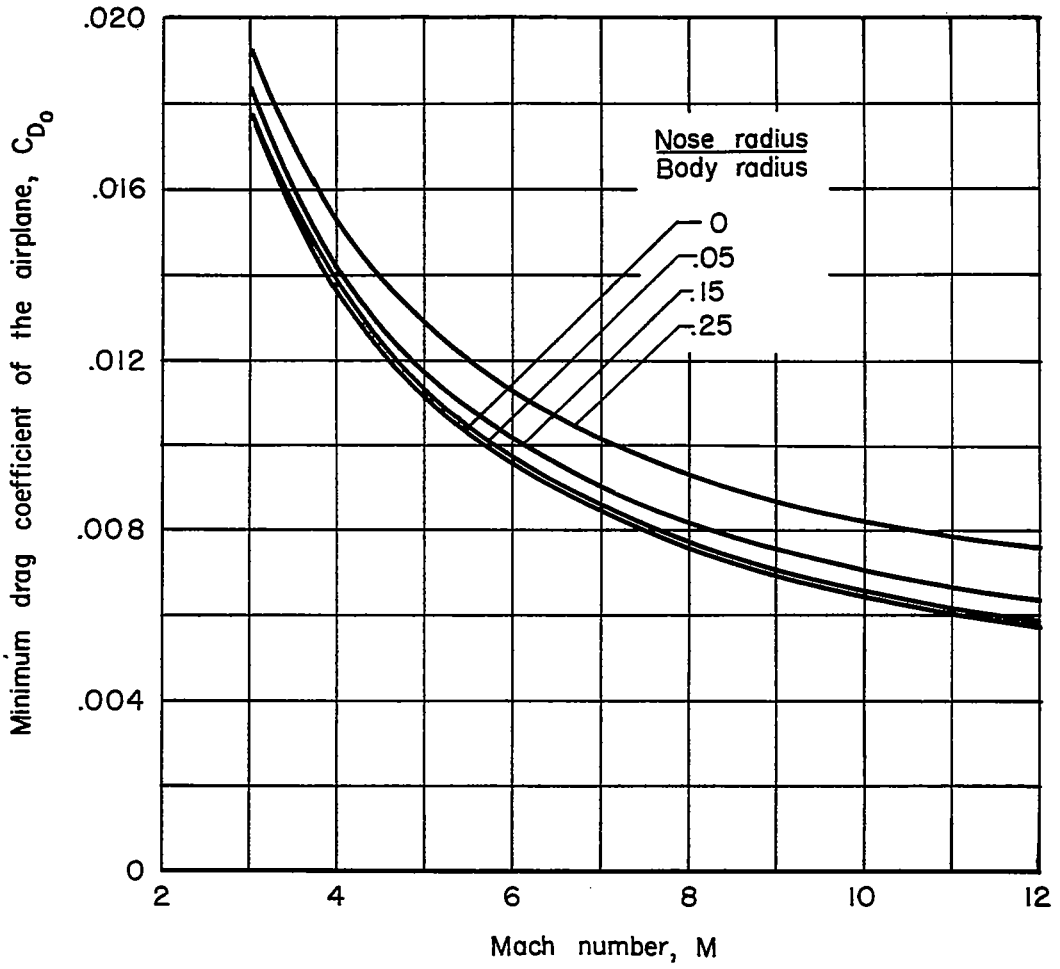

(c) Effect of blunting the fuselage tip.

Figure 8. - Concluded.

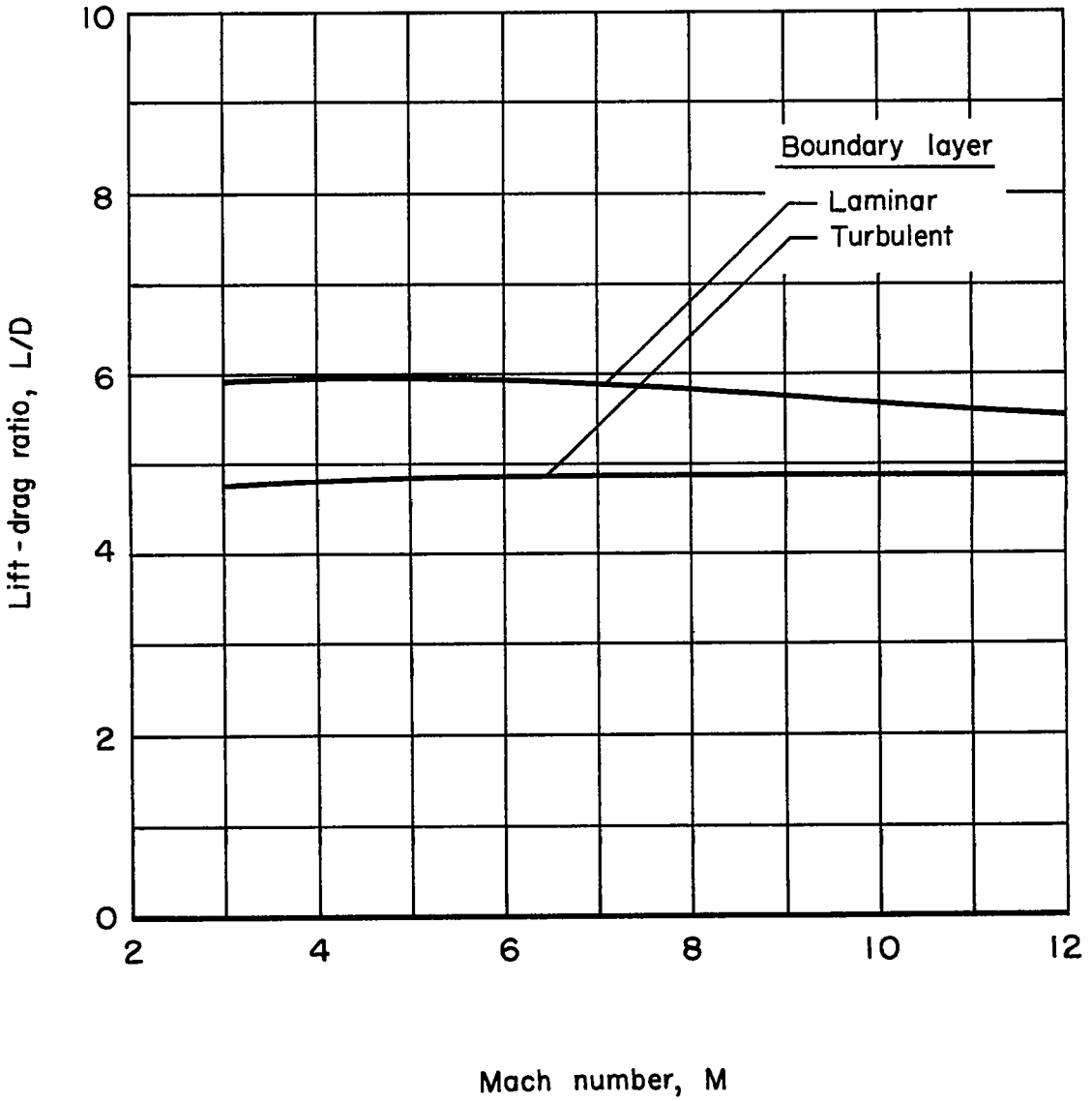

Figure 9. - Estimated lift - drag ratios of the example airplane.

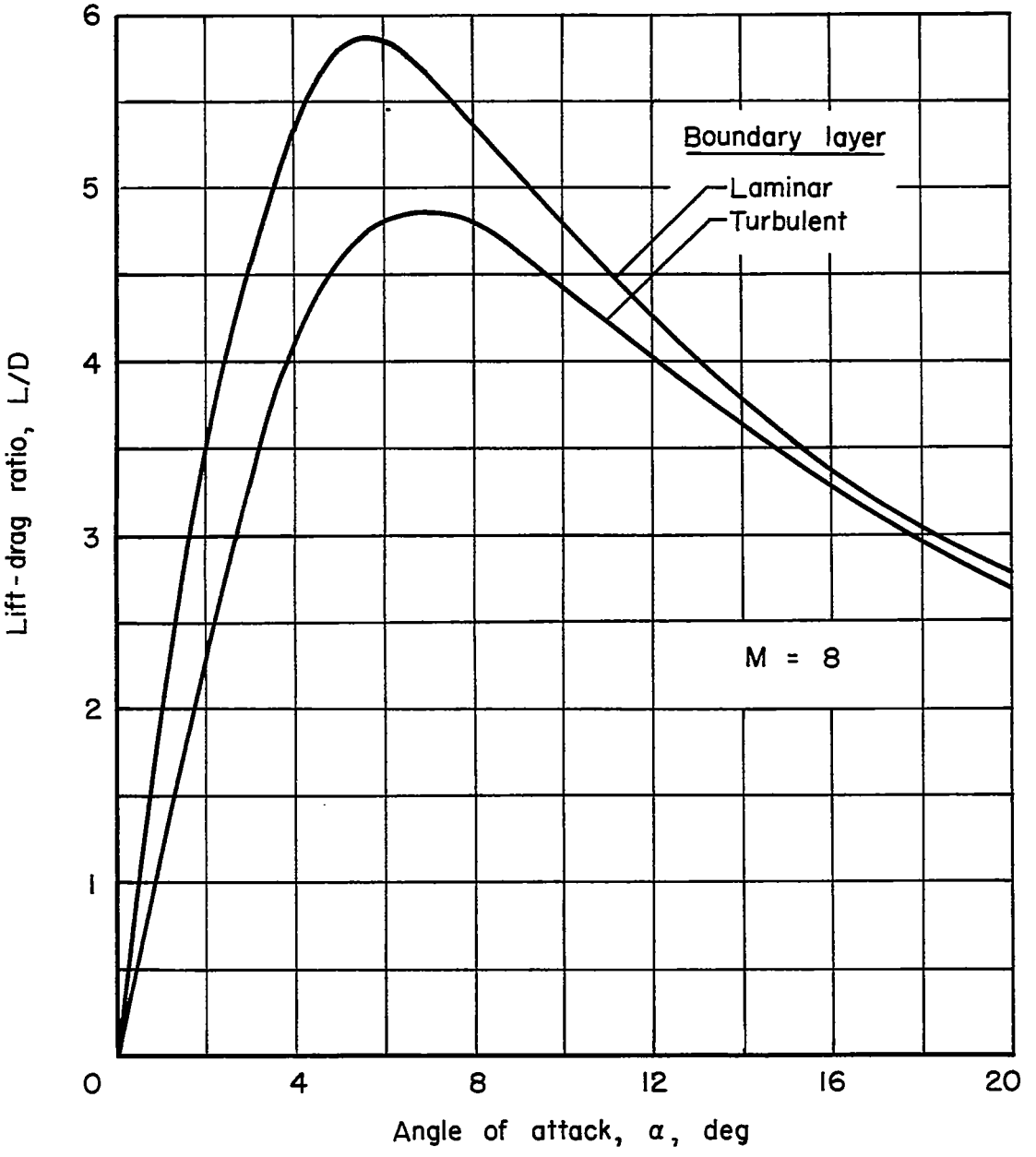

Figure 10. - Variation of estimated lift - drag ratio of example airplane with angle of attack.

[redacted]

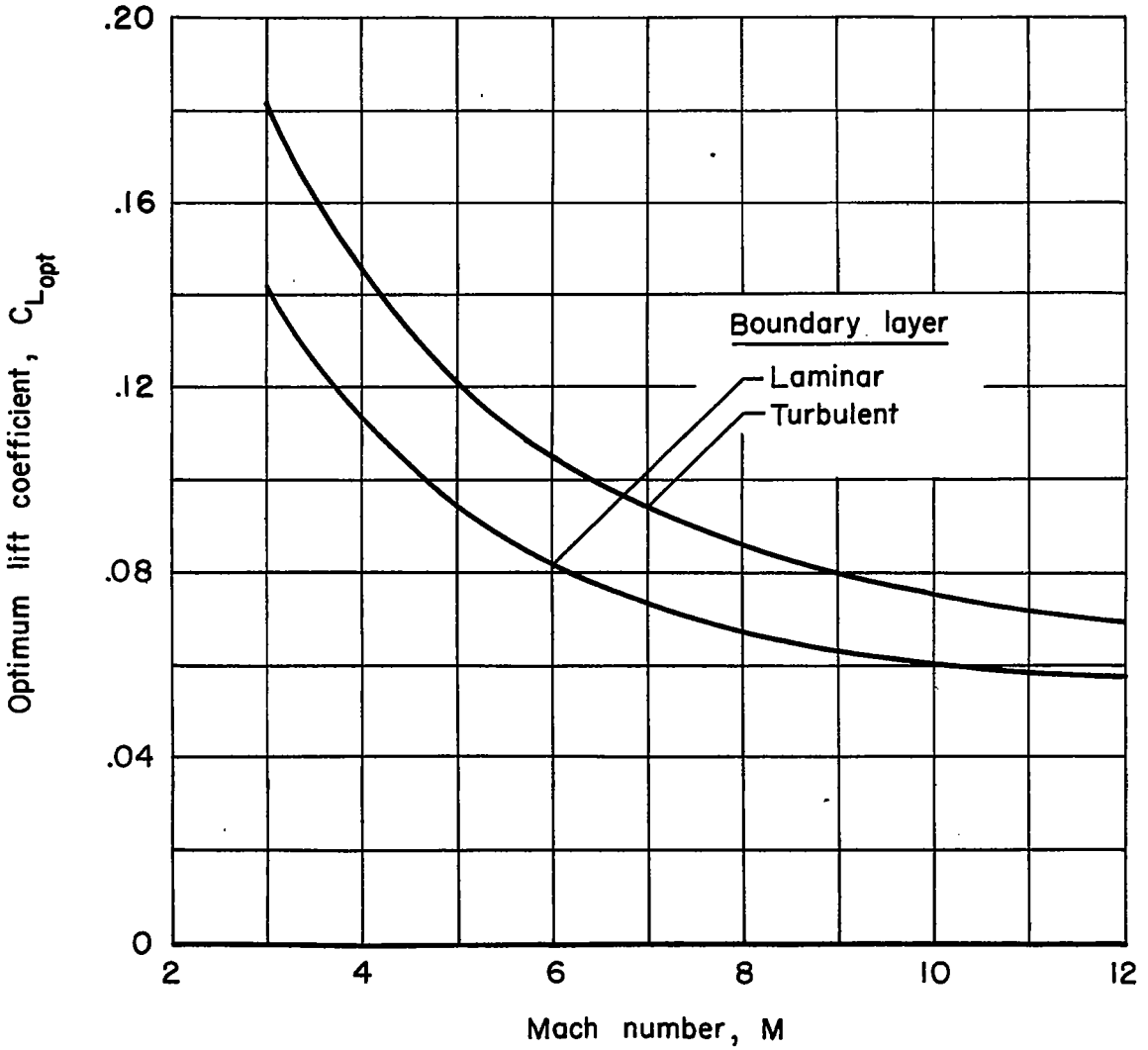

Figure 11. - Optimum lift coefficients of example airplane.

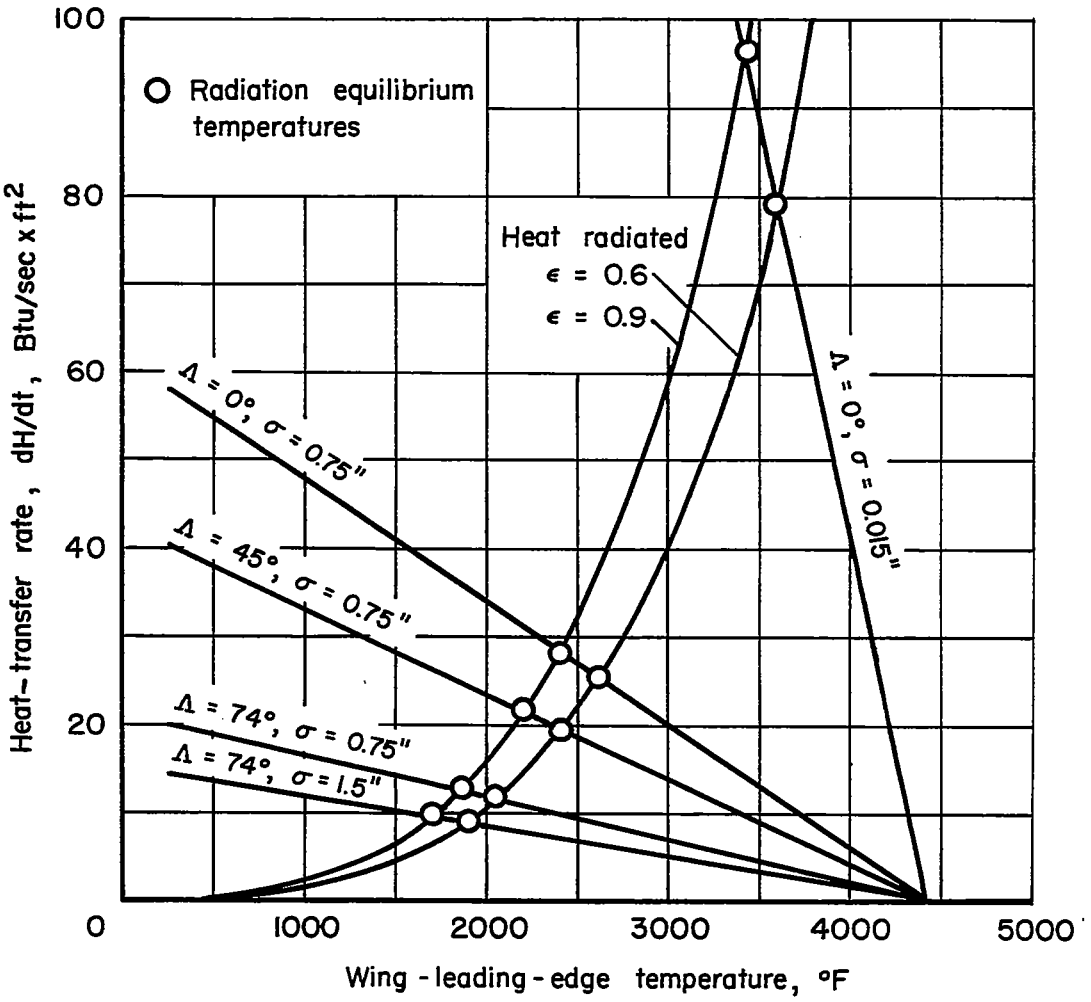

Figure 12. - Wing-leading-edge heating rates at M = 7, 120,000 feet altitude.

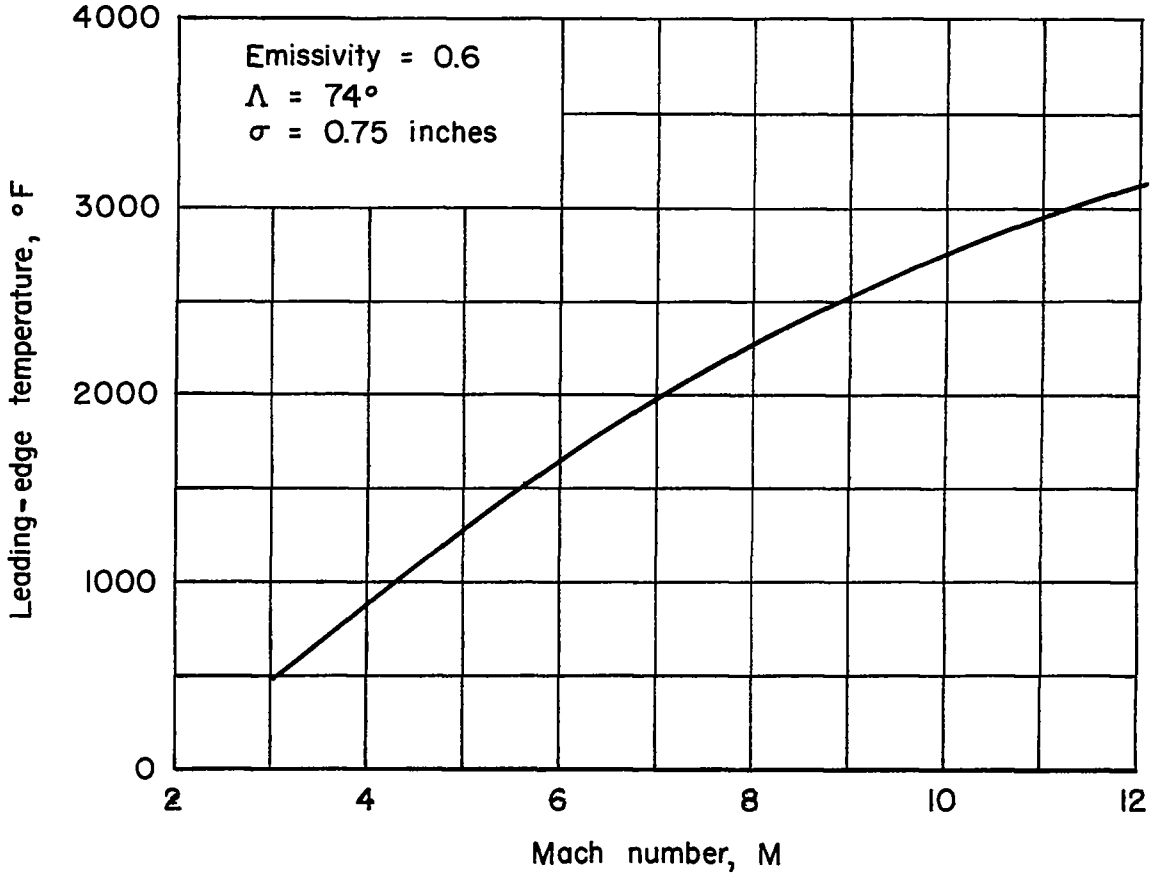

Figure 13. - Radiation equilibrium temperature at leading edge of example airplane.

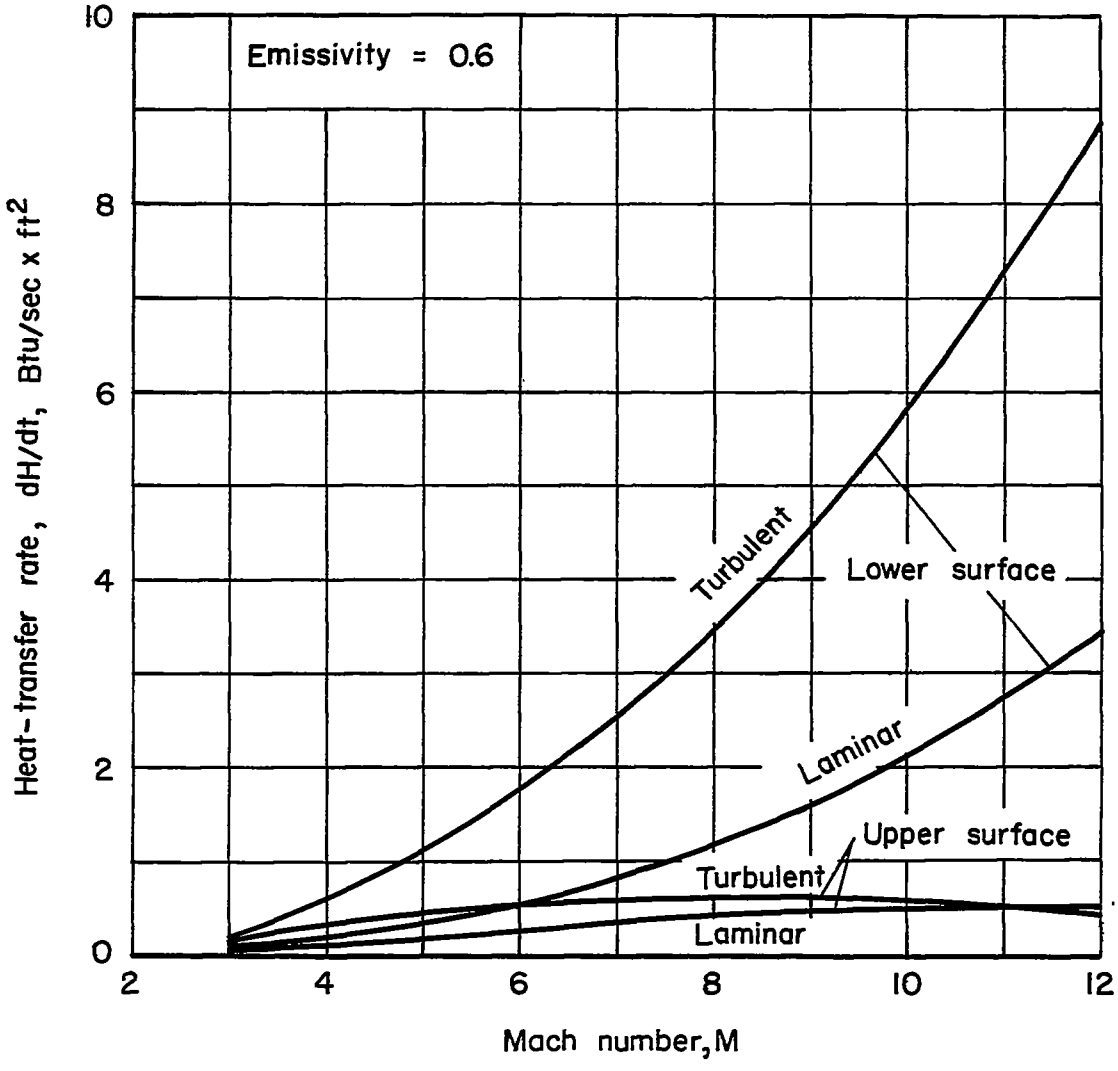

Figure 14. - Average rates of heat transfer to wing of example airplane at radiation equilibrium.

[redacted]

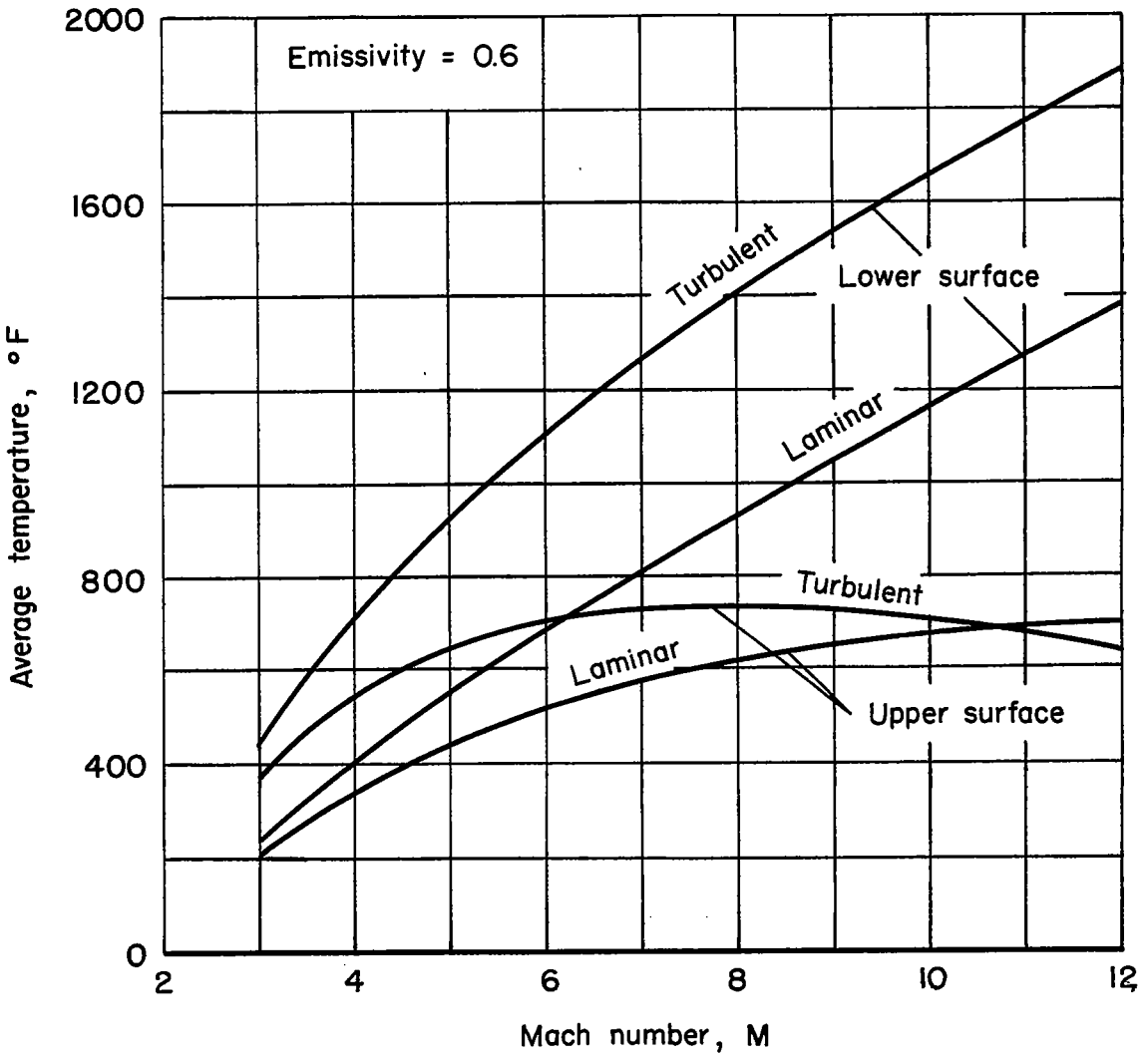

Figure 15. - Average temperatures of the wing surfaces of example airplane at radiation equilibrium.

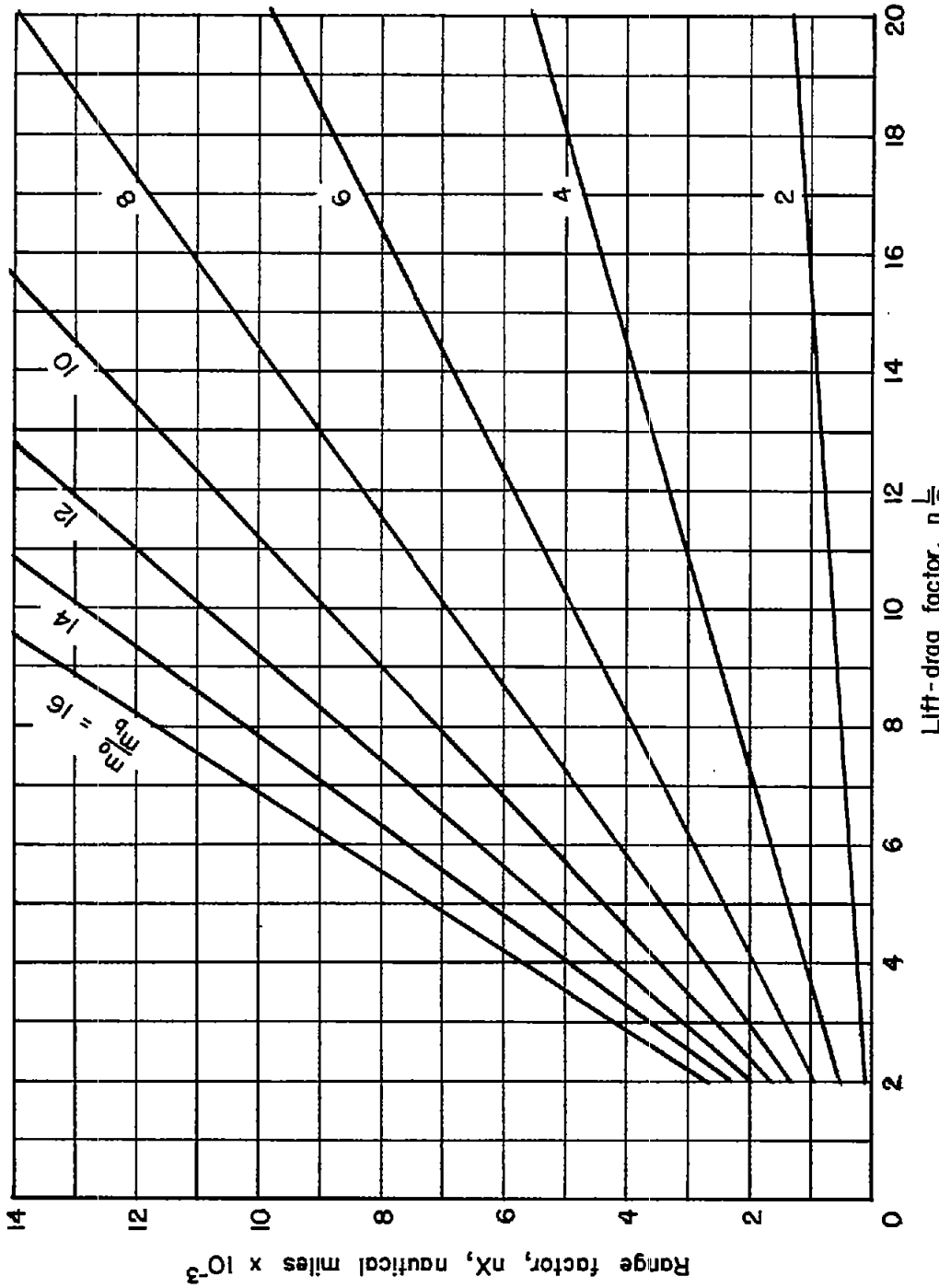

Figure 16. - Range as a function of mass ratio and lift-drag ratio.

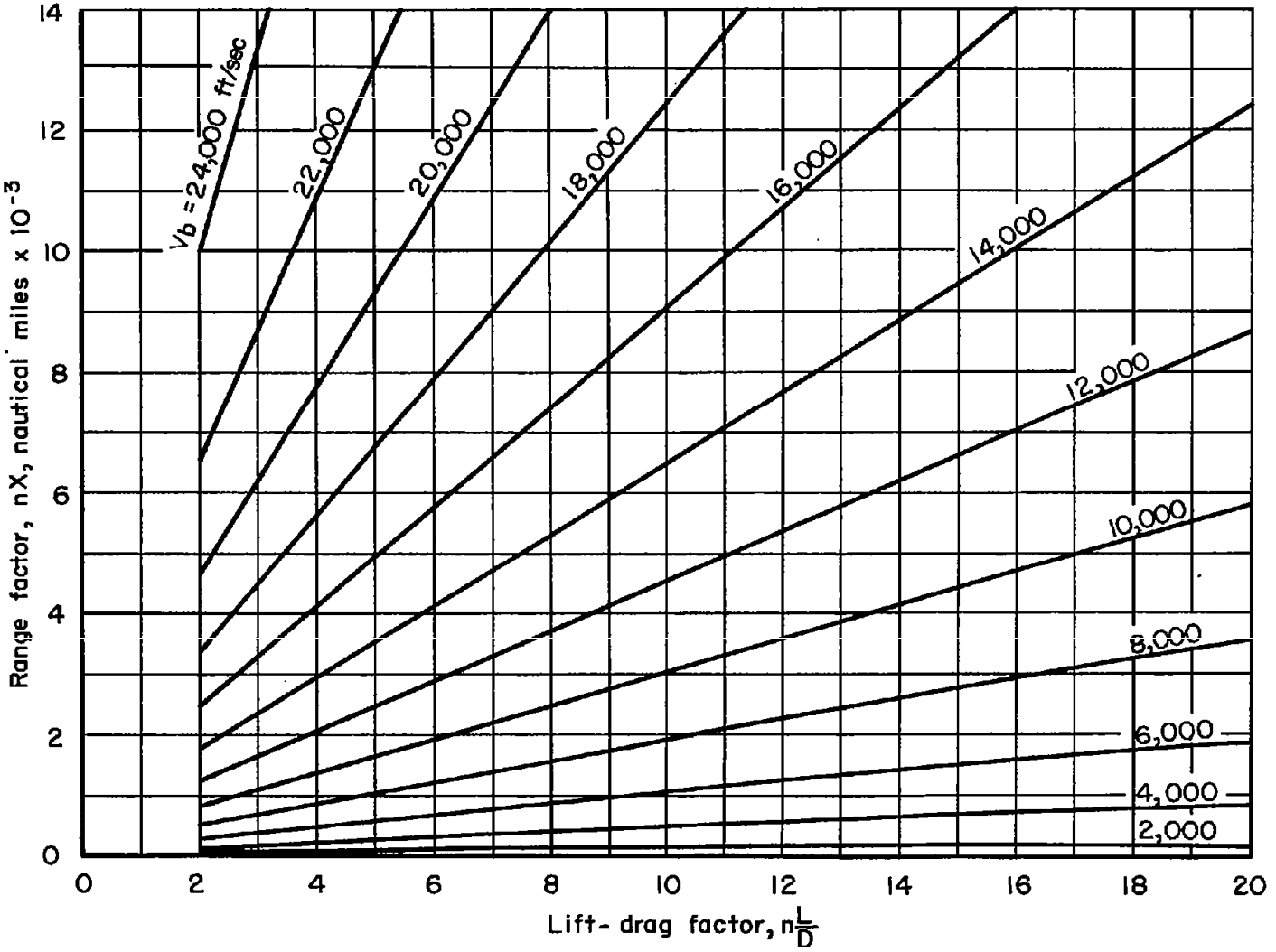

Figure 17.- Range as a function of "Burnout" speed and lift-drag ratio.